Received: 31 July 2023 | Revised: 25 January 2024 | Accepted: 4 February 2024

DOI: 10.1002/hipo.23602

RESEARCH ARTICLE

WILEY

Comparison of histological delineations of medial temporal lobe cortices by four independent neuroanatomy laboratories

Anika Wuestefeld[1] | Hannah Baumeister[2] | Jenna N. Adams[3] | Robin de Flores[4] | Carl J. Hodgetts[5] | Negar Mazloum-Farzaghi[6,7] | Rosanna K. Olsen[6,7] | Vyash Puliyadi[8] | Tammy T. Tran[9] | Arnold Bakker[10] | Kelsey L. Canada[11] | Marshall A. Dalton[12] | Ana M. Daugherty[11,13] | Renaud La Joie[14] | Lei Wang[15] | Madigan L. Bedard[16] | Esther Buendia[17] | Eunice Chung[18] | Amanda Denning[18] | María del Mar Arroyo-Jiménez[17] | Emilio Artacho-Pérula[17] | David J. Irwin[18] | Ranjit Ittyerah[18] | Edward B. Lee[18] | Sydney Lim[18] | María del Pilar Marcos-Rabal[17] | Maria Mercedes Iñiguez de Onzoño Martin[17] | Monica Munoz Lopez[17] | Carlos de la Rosa Prieto[17] | Theresa Schuck[18] | Winifred Trotman[18] | Alicia Vela[17] | Paul Yushkevich[18] | Katrin Amunts[19,20] | Jean C. Augustinack[21] | Song-Lin Ding[22] | Ricardo Insausti[17] | Olga Kedo[19] | David Berron[2] | Laura E. M. Wisse[23]

Correspondence
Hannah Baumeister, German Center for Neurodegenerative Diseases (DZNE), Magdeburg, Germany.
Email: hannah.baumeister@dzne.de

Laura E. M. Wisse, Department of Diagnostic Radiology, Lund University, Lund, Sweden.
Email: lemwisse@gmail.com

Funding information
National Institutes of Health, Grant/Award Numbers: R01-AG070592, P01AG066597, P30AG072979, RF1 AG056014, R01AG057672, RF1AG072056; Wenner-Gren Foundation, Grant/Award Number: ESh2020-002; National Institute on Aging, Grant/Award Numbers: F32AG074621, F32AG071263; Alzheimer Society of Canada, Grant/Award Number: AARFD-21-852597; Horizon 2020 Framework Programme, Grant/Award Number: 945539; Intramural UCLM grant,

Abstract

The medial temporal lobe (MTL) cortex, located adjacent to the hippocampus, is crucial for memory and prone to the accumulation of certain neuropathologies such as Alzheimer's disease neurofibrillary tau tangles. The MTL cortex is composed of several subregions which differ in their functional and cytoarchitectonic features. As neuroanatomical schools rely on different cytoarchitectonic definitions of these subregions, it is unclear to what extent their delineations of MTL cortex subregions overlap. Here, we provide an overview of cytoarchitectonic definitions of the entorhinal and parahippocampal cortices as well as Brodmann areas (BA) 35 and 36, as provided by four neuroanatomists from different laboratories, aiming to identify the rationale for overlapping and diverging delineations. Nissl-stained series were acquired from the temporal lobes of three human specimens (two right and one left hemisphere). Slices (50 μm thick) were prepared perpendicular to the long axis of the hippocampus spanning the entire longitudinal extent of the MTL cortex. Four neuroanatomists annotated

Anika Wuestefeld and Hannah Baumeister contributed equally to this work.

David Berron and Laura E. M. Wisse contributed equally to this work.

For affiliations refer to page 256

Grant/Award Number: GRIN 31097; MultiPark - A Strategic Research Area at Lund University; Canadian Institutes of Health Research, Grant/Award Number: CIHR PJT162292; Biotechnology and Biological Sciences Research Council, Grant/Award Number: BB/V010549/1; Alzheimer's Association; Marcus Wallenbergs Stiftelse för Internationellt Vetenskapligt Samarbete, Grant/Award Number: 2020.0004

MTL cortex subregions on digitized slices spaced 5 mm apart (pixel size 0.4 μm at 20× magnification). Parcellations, terminology, and border placement were compared among neuroanatomists. Cytoarchitectonic features of each subregion are described in detail. Qualitative analysis of the annotations showed higher agreement in the definitions of the entorhinal cortex and BA35, while the definitions of BA36 and the parahippocampal cortex exhibited less overlap among neuroanatomists. The degree of overlap of cytoarchitectonic definitions was partially reflected in the neuroanatomists' agreement on the respective delineations. Lower agreement in annotations was observed in transitional zones between structures where seminal cytoarchitectonic features are expressed less saliently. The results highlight that definitions and parcellations of the MTL cortex differ among neuroanatomical schools and thereby increase understanding of why these differences may arise. This work sets a crucial foundation to further advance anatomically-informed neuroimaging research on the human MTL cortex.

KEYWORDS
Brodmann area 35, Brodmann area 36, entorhinal cortex, harmonization, neuroimaging, parahippocampal cortex, parahippocampal gyrus, segmentation

1 | INTRODUCTION

The medial temporal lobe (MTL) cortex is located adjacent to the hippocampus and comprises the ambient and parahippocampal gyri as well as, in some definitions, the fusiform gyrus (Ding & Van Hoesen, 2010; Figure 1a). The MTL is not only crucial for memory (Eichenbaum et al., 1994; Ritchey et al., 2015; Squire & Zola-Morgan, 1991) but also for olfaction, attention, spatial navigation, and social cognition (Gottfried, 2010; Hannula & Duff, 2017; Iizuka et al., 2021; Levy et al., 1997). Clinically, the MTL cortex is a key brain region for neurodegenerative processes, caused by a variety of factors such as Alzheimer's disease pathology (Berron et al., 2021; Braak & Braak, 1991; Lace et al., 2009; Llamas-Rodríguez et al., 2022; Matej et al., 2019; Yushkevich, Muñoz López, et al., 2021) or limbic-predominant age-related transactive response DNA binding protein-43 encephalopathy (TDP-43; Matej et al., 2019; Nelson et al., 2019; Yushkevich, Muñoz López, et al., 2021). In each of these conditions, early pathological changes occur in the MTL cortex and are related to emerging amnestic symptoms (Braak & Braak, 1991; Nelson et al., 2012, 2019).

It is important to mention that the MTL cortex (incorporating the ambient, parahippocampal, and fusiform gyri) is not a single homogeneous entity, but rather exhibits high variance in cytoarchitecture. Its anteromedial portion comprises three-layered, allocortical structures of the hippocampus, whereas its outmost lateral subregions exhibit the key characteristics of six-layered isocortex (Braak & Braak, 1995; Ding & Van Hoesen, 2010; Filimonoff, 1947; Insausti et al., 1995, 2017; Van Hoesen et al., 2000). This heterogeneous composition has led neuroanatomists to distinguish various subregions of the human MTL cortex with partially overlapping terminology.

In their seminal cytoarchitectonic brain maps, Brodmann (1909) as well as von Economo and Koskinas (1925) established two distinct atlases of the MTL cortex (Figure 1b). On Brodmann's map, it spans Brodmann Area (BA) 28 (*area entorhinalis*), BA34 (*area entorhinalis dorsalis*), BA35 (*area perirhinalis*), and BA36 (*area ectorhinalis*). The term entorhinal cortex (ERC) has been used as an umbrella term for BA28 and BA34, corresponding to its portions located on the anterior parahippocampal and ambient gyri, respectively (Insausti et al., 1995, 2019). The perirhinal cortex is anteriorly, laterally, and posteriorly adjacent to the ERC and corresponds to BA35. BA36 has previously been referred to as ectorhinal cortex (Augustinack, Huber, et al., 2013; Brodmann, 1909; Van Hoesen et al., 2000) but has also been grouped with BA35 under the term perirhinal cortex (Ding & Van Hoesen, 2010; Insausti et al., 2017; Kivisaari et al., 2012). Importantly, Brodmann's map is clearer in the anterior MTL cortex but less so in its posterior portion, also referred to as parahippocampal cortex (PHC; not to be confused with parahippocampal gyrus, which is the gross anatomical term for the gyrus adjacent to the hippocampus). In fact, Brodmann (1909) proposed a region termed BA48 (*area retrosubicularis*) to border BA35 posteriorly. However, Brodmann was unable to reliably identify this region in humans, and thus it was not included in Brodmann's final neuroanatomical atlas, leaving some ambiguity in the posterior MTL cortex. If corresponding to any BA, the PHC may include some posterior portions of BA36.

The anatomical map established by von Economo and Koskinas (1925) depicts the MTL cortex as areas HA, HB, HC of the *regio hippocampi* (associated with the ERC) and part of TG (TGa) anteriorly (*regio polaris*), as well as regions TH (THa) and TF posteriorly (*regio fusiformis*; Figure 1b). Areas THa and TGa are possible correlates of BA35. THa lies posteromedial to TGa on the crown of the parahippocampal gyrus and adjacent to the parasubiculum, presubiculum, or transsubiculum of the hippocampal formation (Palomero-Gallagher et al., 2020). Region TH extends from the lateral crown of the parahippocampal gyrus to the lateral bank of the collateral sulcus and is laterally bordered by the fusiform region TF (von Economo & Koskinas, 1925). Part of region PH (von Economo & Koskinas, 1929)—a large transitional area spanning the posterior parietal and temporal lobes—has

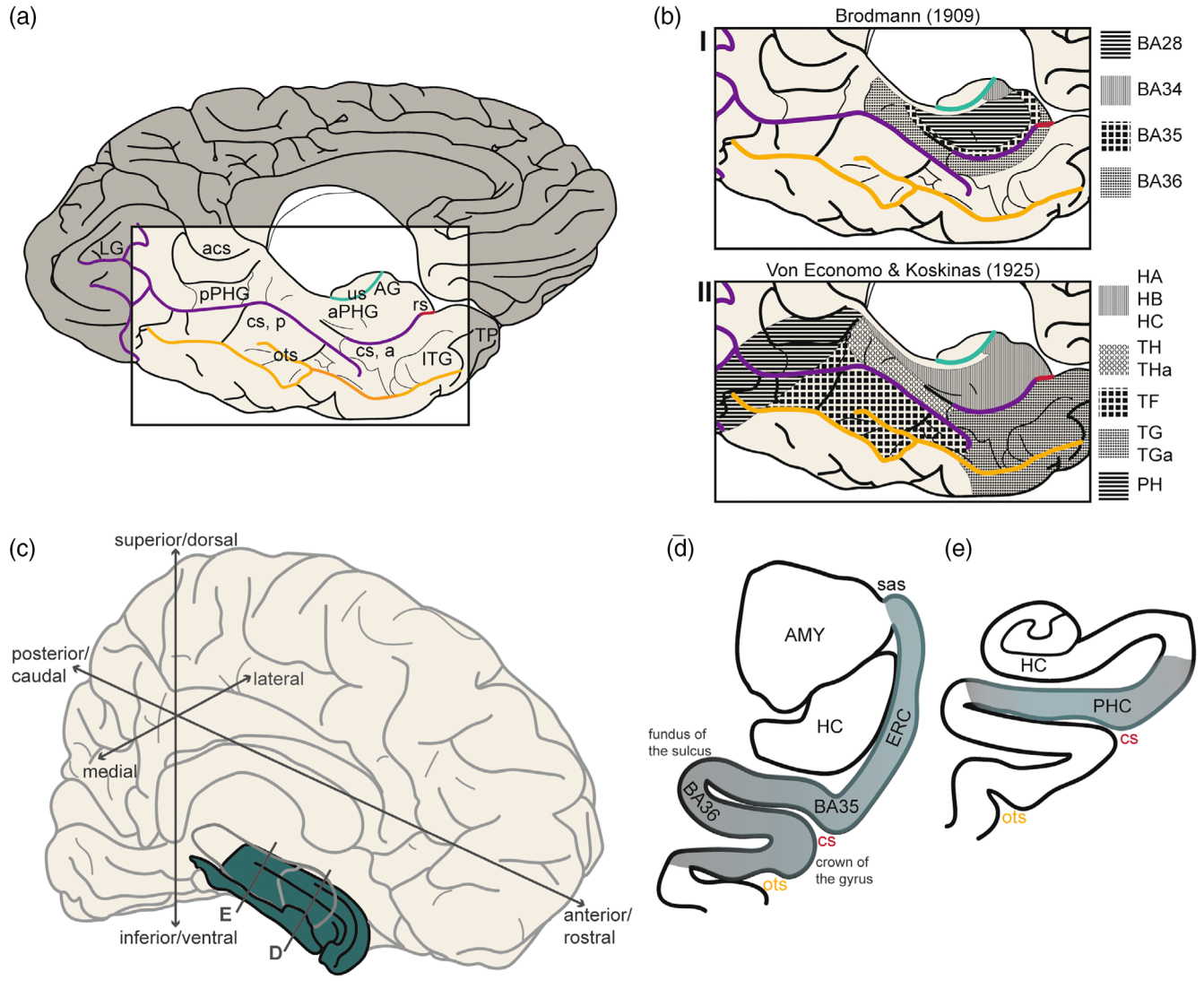

(f)

Gyri	
AG	ambient gyrus
aPHG	anterior para-hippocampal gyrus
ITG	inferior temporal gyrus
pPHG	posterior para-hippocampal gyrus
LG	lingual gyrus
TP	temporal pole

Sulci	
acs	anterior calcarine sulcus
cs	collateral sulcus
	a = anterior
	p = posterior
us	uncal/hippocampal sulcus
ots	occipitotemporal sulcus
rs	rhinal sulcus
sas	sulcus semiannularis

Anatomical structures	
AMY	amygdala
BA35	Brodmann area 35
BA36	Brodmann area 36
ERC	entorhinal cortex
HC	hippocampus
PHC	parahippocampal cortex

FIGURE 1 Overview of the cortical MTL structures investigated in the present study. Panel (a) shows an inferior–medial view of the brain cut at the midline with labels for relevant gyri and sulci. Panel (b) approximates two historical human brain maps (bI: Brodmann, 1909; bII: von Economo & Koskinas, 1925). Panel (c) is a three-dimensional visualization of the MTL cortex (in green) embedded in the left hemisphere indicating important terminology and identifying the approximate position of panels (d) and (e). Panels (d) and (e) visualize the rough position of the MTL cortex subregions investigated in this study. Panel (d) shows an anterior coronal section of the MTL cortex including the ERC and BA 35 and 36 labels. The color gradient indicates certainty of borders (blue: higher agreement, gray: lower agreement). Panel (e) shows a more posterior section of the MTL cortex showing the PHC. Panel (f) explains the abbreviations used in panels (a–e).

been considered part of the PHC as well (Stenger et al., 2022). BA36 may be related to parts of TG and posterior TH (*regio temporo-hippocampica*). Further descriptions of these regions in humans, macaques, and chimpanzees can be found elsewhere (Bailey et al., 1950; Bailey & von Bonin, 1951; von Bonin & Bailey, 1947).

Since the establishment of these first exhaustive neuroanatomical atlases, histological studies have benefitted from methodological advancements (e.g., digitalization and immunohistochemistry) and neuroanatomists have developed and specified these existing brain maps continuously. Such advancements have led to the distinction of

subregions at remarkably detailed levels. For instance, BA35 has been subdivided into BA35a and BA35b based on their distinct cytoarchitecture (Augustinack, Huber, et al., 2013; Ding & Van Hoesen, 2010; Van Hoesen et al., 2000) and several subfields of the ERC have been identified (Behuet et al., 2021; Braak & Braak, 1992; Filimonoff, 1947; Insausti et al., 1995, 2017; Krimer et al., 1997). A multitude of additional parcellations can be found in the extensive literature on nonhuman primates (e.g., Blatt & Rosene, 1998; Insausti et al., 1987; Suzuki & Amaral, 2003). In addition to the improvement of histological methods, histological datasets have grown. In combination with the rise of in vivo neuroimaging techniques, this development has provided crucial insights into interindividual differences in neuroanatomy. For example, it has become apparent that the MTL cortex exhibits great interindividual variation in micro- as well as macrostructure (Augustinack, van der Kouwe, et al., 2013; Ding & Van Hoesen, 2010; Insausti et al., 1998; Ono et al., 1990). In particular, the rhinal and collateral sulci vary in depth and ramifications. Variance in collateral sulcus depth and continuity have been linked to differing gross anatomical locations of MTL cortex subregions (Ding & Van Hoesen, 2010; Insausti et al., 1998; Taylor & Probst, 2008). Considering the different histories and subsequent development of anatomical studies, it is unsurprising that neuroanatomical schools rely on different definitions of the MTL cortex and its subregions.

The described micro- and macroanatomical variance within the MTL cortex poses a challenge to researchers who aim to distinguish MTL cortex subregions on magnetic resonance imaging (MRI) scans for a wide range of research applications. However, accurate delineations are crucial as MTL cortex subregions show distinct involvement in processes of basic and clinical neuroscientific interest. For instance, it has been proposed that the perirhinal cortex (here referring to BA35 and BA36) and the PHC belong to distinct networks of cognition (Maass et al., 2015; Navarro Schröder et al., 2015; Ritchey et al., 2015; Squire & Zola-Morgan, 1991; but also note Doan et al., 2019), making their accurate distinction critical. With regard to neurodegeneration, subregions of the MTL cortex are differently targeted by pathology and healthy aging (Llamas-Rodríguez et al., 2022; Stark & Stark, 2016). The importance of accurate MTL cortex parcellation becomes evident in the case of Alzheimer's disease, in which early neurofibrillary tau tangles are located in the transentorhinal region, likely corresponding to BA35 (Braak & Braak, 1985, 1991; Ding & Van Hoesen, 2010; Insausti et al., 1998).

While the neuroanatomical investigation of the MTL cortex is progressing, proposed parcellations and definitions of subregions used for neuroimaging studies continue to diversify (Yushkevich, Amaral, et al., 2015). This diversity may stem either from inter-individual neuroanatomical variability or, as segmentation protocols are informed by different neuroanatomical laboratories, from diverging definitions of brain structures. To clarify the influence of the latter, it is necessary to examine the overlap of different neuroanatomical laboratories when delineating brain structures on histological samples. Here, we provide an overview of the cytoarchitectonic definitions of MTL cortex subregions as provided by four neuroanatomists (J.C.A., R.I., O.K., and S.L.D.), based at four different laboratories. We focus on subregions ERC, BA35, BA36, and PHC (Figure 1c–e), as this parcellation is commonly found in the neuroanatomical literature and has been translated into MTL cortex segmentation protocols for MRI (Augustinack, Huber, et al., 2013; Berron et al., 2017; Fischl et al., 2009; Insausti et al., 1998; Xie et al., 2019; Yushkevich, Pluta, et al., 2015). We additionally compare annotations of these subregions on histological sections of the same three specimens for all neuroanatomists. The insights from this detailed analysis of MTL cortex subregional delineations will provide a basis for the ongoing Hippocampal Subfields Group's effort to develop a harmonized segmentation protocol for MTL cortex subregions to be used for in vivo MRI (Olsen et al., 2019; Wisse et al., 2017; Yushkevich, Amaral, et al., 2015). Moreover, the present study will benefit human neuroimaging studies of the MTL cortex in a broader sense by allowing more precise localization of MTL cortex structures, more valid interpretation of results, and higher comparability across studies.

2 | MATERIALS AND METHODS

2.1 | Specimens

Three human MTL specimens, two from the Human Neuroanatomy Laboratory (HNL) at University of Castilla-La Mancha (UCLM, Albacete, Spain) and one from the Center for Neurodegenerative Disease Research at the University of Pennsylvania (UPenn, Philadelphia, USA), were used. Human brain specimens were obtained in accordance with the UCLM Ethical Clinical Committee and the University of Pennsylvania Institutional Review Board guidelines. Written consent was obtained in all HNL cases. Pre-consent during life and, in all cases, next-of-kin consent at death was given at UPenn. The three specimens were selected to represent both sexes, both hemispheres, a wide age range, cases with and without reported neurodegenerative disease diagnosis, and a broad variability in depth and length of the collateral sulcus to evaluate the location of MTL cortical fields in relationship to macrostructural landmarks. Table 1 provides demographic and diagnostic details of the selected specimens. Note that for ease of interpretation, the left hemisphere specimen (specimen 2) was mirrored in all figures to match the orientation of the other specimens.

2.2 | Hemisphere preparation and diagnostic pathology

At UCLM, fixation was performed by intracarotid perfusion with the brain in the skull (in situ; Insausti et al., 2023) before brain removal at autopsy with 4% paraformaldehyde in 0.1 M phosphate buffer. At UPenn, brain specimens were fixed in 10% neutral buffered formalin after autopsy. At both centers, hemispheres were fixed for at least 4 weeks. The opposite hemisphere was sampled for diagnostic pathology according to the National Institute of Aging and Alzheimer's Association (NIA-AA) protocol (Hyman et al., 2012). After hemisphere fixation, an intact tissue block containing the full temporal lobe was dissected and placed in the fixative for 7 Tesla (T) MRI scanning.

TABLE 1 Demographic, diagnostic, and neuropathological information of the three specimens.

	Specimen 1	Specimen 2	Specimen 3
Age (years)	90+[a]	66	83
Sex	Male	Female	Female
Postmortem interval (hours)	6	9	4
Hemisphere annotated	Right	Left	Right
Collateral sulcus	Deep and continuous	Deep and discontinuous	Shallow and discontinuous
Diagnosis	Low ADNC	Unremarkable brain	Low ADNC, PSP
Neuropathological staging			
A:B:C score[b]	A1:B1:C0	A0:B1:C0	A1:B0:C0
NFT	Braak II	Braak II	Braak 0; 3+ tau (PSP)

Note: Diagnosis and neuropathological staging were derived from contralateral sampling.
Abbreviations: A, amyloid score based on Thal phases for amyloid deposits; ADNC, Alzheimer's disease neuropathologic change; B, neurofibrillary tangle stage, modified from Braak and Braak (1991); C, CERAD neuritic plaque score; NFT, neurofibrillary tangles (AT8 staining); PSP, progressive supranuclear palsy.
[a]As age over 89 is considered protected health information in the US, the exact age of this specimen is not disclosed.
[b]Pathology severity rating (A:B:C score; see Hyman et al., 2012).

2.3 | Serial histology and immunohistochemistry

Beginning at the temporal pole, specimens were cut coronally following the plane of the 7 T MRI into four parallel 20 mm thick blocks using a custom three-dimensional mold that was generated from a postmortem 7 T MRI. Using dry ice, cryoprotected blocks were frozen and serially sectioned into 50 µm sections using a sliding microtome coupled to a freezing unit after digital block-face images were taken.

Every resulting section was collected in a freezing protectant solution. Every 10th section was immediately mounted and Nissl-stained with thionin for cytoarchitectonic analysis, resulting in a 0.5 mm gap between adjacent stained sections. The remaining tissue was saved for further use. Every 20th section (1 mm gap between stained sections) was stained using AT8, a phosphorylated tau antibody immunohistochemistry stain. All sections were counterstained with lower intensity thionin. Sections were mounted on glass slides, digitally scanned, and uploaded to a cloud-based digital histology archive which supports anatomical labeling (see Appendix S1).

2.4 | Histological annotations

For the purposes of this study, Nissl-stained sections 5 mm apart were selected to be annotated, resulting in a total of 15–16 digitized slices (pixel size 0.4 µm at 20× magnification) annotated per specimen. This selection of sections aimed to balance workload for the neuroanatomists while ensuring thorough coverage of the MTL cortex subregions. First, after receiving instruction on the digital annotation tool (see Appendix S1), annotations were completed independently by each neuroanatomist (J.C.A., O.K., R.I., S.L.D.). Second, J.C.A., O.K., and R.I. attended a Hippocampal Subfields Group working group meeting in June 2022 during which their annotations and definitions of MTL cortex subregions were discussed. At this meeting each region was discussed individually, comparing the histological annotations of the neuroanatomists—focusing on the main discrepancies and similarities—and clarifications on the reasoning of specific delineations and definitions were provided. Third, J.C.A., O.K., and S.L.D. received access to the full range of serial histology slices to further inform their annotations and potentially adjust them, which two of them completed. R.I. had access to the full range of serial histology slices from the beginning, as part of another project. Fourth, all four neuroanatomists were consulted for follow-up clarifications and asked to provide the seminal cytoarchitectonic features per region that they used to inform their annotations. Assessments of agreement among neuroanatomists were performed per subregion in a qualitative manner.

3 | RESULTS

All neuroanatomists determined the borders of ERC, BA35, BA36, and PHC, with finer subdivisions of these subregions made by some neuroanatomists following common practices in their respective laboratories. The following sections first provide a short introduction to the key cytoarchitectonic concepts that informed the neuroanatomists' annotations. Next, the cytoarchitectonic features, definitions, and parcellations of each MTL cortex subregion, as provided by the neuroanatomists, are described and compared.

3.1 | Key cytoarchitectural concepts used for MTL cortex parcellation

Cytoarchitectonic features such as neuronal size, type, organization, and packing density in the different cellular layers were the main source of information used for annotations. At times, some neuroanatomists additionally referred to gross anatomical landmarks in their justifications of border placement. Table 2 provides definitions of key

TABLE 2 Key cytoarchitectonic concepts used for the delineation of the entorhinal cortex, Brodmann areas 35 and 36, and the parahippocampal cortex.

Concept	Definition	Cortex type	Definition
Granularity		Allocortex	Three-layered cortex
Agranular cortex	Lacks granule cell bodies	Periallocortex	Six-layered[a] agranular cortex
Dysgranular cortex	Exhibits few loosely packed granule cells	Proisocortex	Six-layered dysgranular cortex in which not all isocortical features are clearly expressed
Granular cortex	Prominent and densely packed layer of granule cells	Isocortex	Six-layered granular cortex showing an organized internal and external granule cell layer
Lamina dissecans	Thoroughly agranular layer splitting the cortex in two halves		
Layer II cell islands	Darkly stained stellate cells occurring in clusters in the ERC		
Columnarity	Columnar organization of cortical cells perpendicular to the cortical layers II and/or III		
Internal vs. external layers	Deep layers close to white matter vs. superficial layers close to pial surface		

Abbreviation: ERC, entorhinal cortex.
[a]Terminology describing periallocortical cell layers may differ from terminology used for (pro-)isocortical regions (see, e.g., Ding & Van Hoesen, 2010), while this paper uses consistent terminology. Additionally, note that the (peri-)allocortical layers are not homologous to the layers of the isocortex, since the (peri-)allocortical layers are evolutionarily different from those of the isocortex.

cytoarchitectonic concepts that were relevant for the delineation of MTL cortex subregions.

An important concept was granularity, which here focuses on the number and organization of granule cells in layer IV (or the equivalent in ERC; see Table S1) of the cortex (Figure 2). The degree of granularity can range from the complete lack of granule cell bodies (agranular cortex) to the presence of few, loosely arranged granule cells (dysgranular cortex), to the dense packing of highly organized granule cells (granular cortex; Brodmann, 1909; Insausti et al., 2017; von Economo & Koskinas, 1925). Changes in granularity are one of the main distinguishing features of MTL cortex subregions which reflect the transition from periallocortex (agranular), proisocortex (dysgranular), to isocortex (granular; Brodmann, 1909; Ding & Van Hoesen, 2010; Insausti et al., 2017; von Economo & Koskinas, 1925). A cytoarchitectonic feature that can coincide with an absent granule cell layer IV is the *lamina dissecans*. It is a thoroughly cell-sparse, agranular layer and, in the MTL cortex, specific to the ERC. It divides the cortex into two halves or, if two *laminae dissecans* are present, encloses a small layer of large pyramidal cells between two cell-free layers (layers Va and Vb in Insausti et al., 1995; see also Insausti et al., 2017; Stephan, 1975). Another concept used to parcellate MTL cortex subregions is the presence or absence of layer II cell islands (Figure 2a). These prominent clusters of large stellate cells, also termed pre-α cell islands (Braak & Braak, 1985), are most prominent in the ERC (Ding & Van Hoesen, 2010; Insausti et al., 1995; Schön et al., 2022). Lastly, columnarity is a feature that is differently expressed throughout layer II and/or III in different subregions of the MTL cortex (Figure 2b). It can be defined as the irregular arrangement of cells, forming cell accumulations that are oriented perpendicular to the pial surface and are separated by cell-sparse parts.

3.2 | Cytoarchitectonic and gross anatomy features of MTL cortex subregions

Annotations of all neuroanatomists primarily relied on cytoarchitectonics, not on the gross anatomical appearance of the MTL cortex. Only one neuroanatomist referred to gross anatomical hallmarks as a relevant source of information for border definition, as described previously (Ding & Van Hoesen, 2010). Table 3 provides a short overview of each structure's core cytoarchitectonic features as stated by the neuroanatomists. A more detailed overview can be found in Table 4, which also highlights points of agreement and disagreement among the neuroanatomists. Although the neuroanatomists agreed upon the presence of these features, they were weighed differently by the neuroanatomists when making boundary placement decisions.

3.2.1 | Entorhinal cortex

Among all subregions, the cytoarchitectonic definition of the ERC exhibited the highest agreement among neuroanatomists. The ERC was consistently referred to as a six-layered, periallocortical structure (Augustinack, Huber, et al., 2013; Ding & Van Hoesen, 2010; Insausti et al., 1995, 1998). Compared with the adjacent BA35, its cells are overall relatively large. Layer II comprises large stellate cells (also referred to as fan cells; Tahvildari & Alonso, 2005; see also Nilssen et al., 2018; Vandrey et al., 2020) that cluster to form cell islands (Braak & Braak, 1985; Rose, 1927; Figure 2a). These layer II cell islands are highly characteristic for the ERC, though they are most prominently expressed in its posteriolateral extent (Behuet et al., 2021).

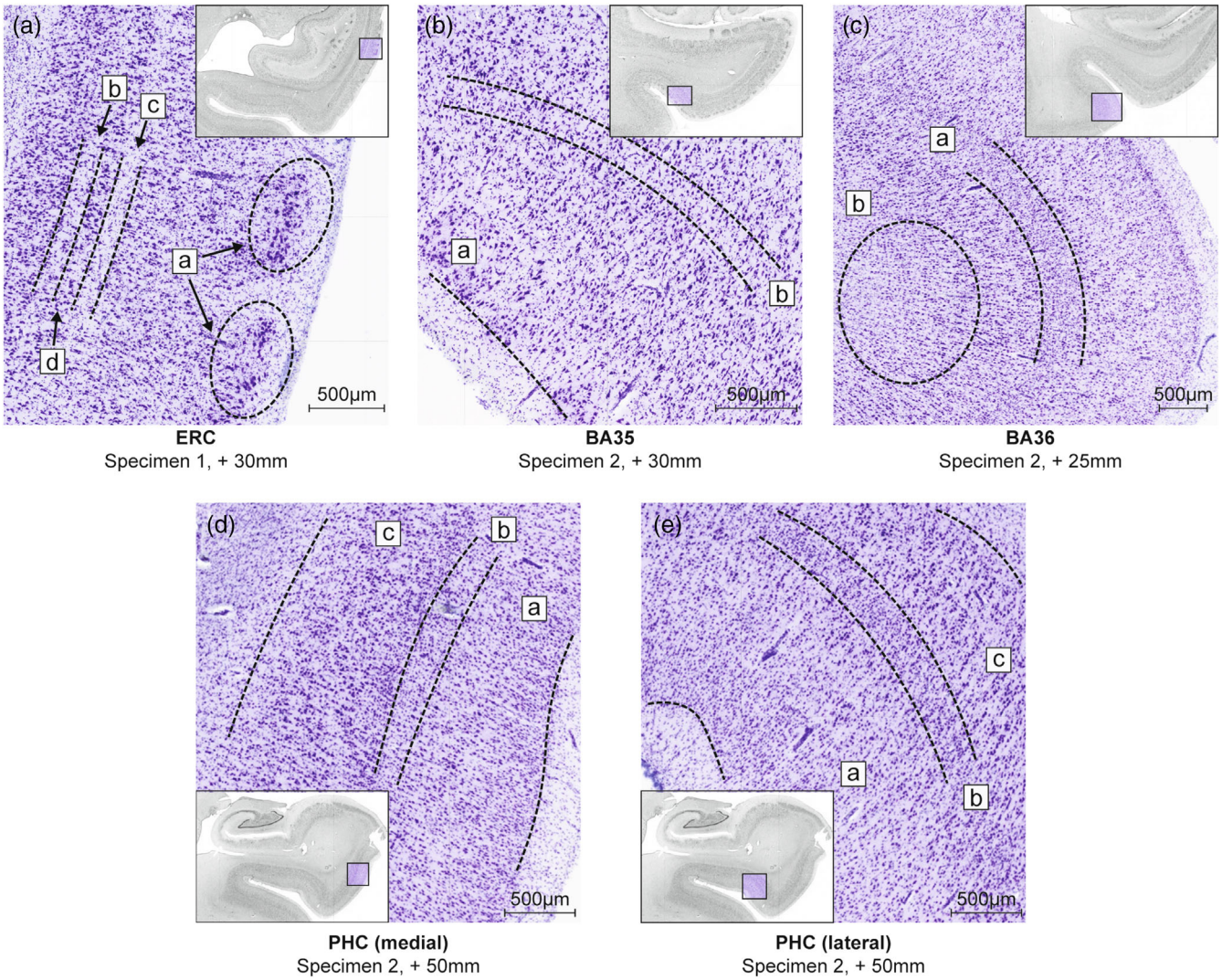

FIGURE 2 Examples for seminal features for each of the annotated MTL cortex subregions. Millimeters indicate distance from the temporal pole. All displayed examples were annotated as the indicated subregions by all neuroanatomists. Panel (a) shows a section of ERC. Seminal features include layer II cell islands (a) and an internal (b) and external (c) *lamina dissecans*, which enclose a dense layer of pyramidal cells (d; see Table S1 for differences in nomenclature). Panel (b) shows a section that was annotated BA35 and shows a columnar organization of layers II and III (a) and an incipient dysgranular layer IV (b). Panel (c) displays a section annotated BA36. It features the region's thick layer IV, but with loosely organized cells (a) and a fluent transition of layer VI with the white matter (b). PHC was described as a highly heterogeneous region, thus two examples are shown. A more medial section of PHC is shown in Panel (d), with layer II gradually transitioning into layer III (a), an incipient dysgranular layer IV (b), in which scarce granular cells are intermingled with cells from the neighboring layers, and homogenous layers V and VI (c). Features in more lateral parts of the PHC, as shown in Panel (e), are similar. Note that in contrast with the medial section, layer II and layer III are more distinguishable (a) and layer IV exhibits an almost isocortex-like degree of granularity (b). Still, no clear border between layers V and VI is visible (c). Note that individual annotations often extended further lateral than shown in Panel (e). However, there was no slice in which more lateral sections were annotated PHC by all neuroanatomists. BA, Brodmann area; ERC, entorhinal cortex; PHC, parahippocampal cortex.

Layer III of the ERC is rather thick with pyramidal cells clustered into columns. Neuroanatomists agreed that the ERC is a thoroughly agranular structure with a clearly visible *lamina dissecans*, splitting the cortex into an internal (or deep, between white matter and *lamina dissecans*) and external (or superficial, between pial surface and *lamina dissecans*) principal layer (Braak & Braak, 1985; Insausti et al., 2017; Rose, 1927). In some sections of the ERC, two cell-free layers are formed: an external (sometimes referred to as proper *lamina dissecans*) and an internal cell-free layer (sometimes also referred to as *lamina dissecans*, while not by all neuroanatomists; see Table S1). Note that the terminology used to distinguish cellular layers in the ERC differs from that used in most of the cortex due to ontogenetic differences (Behuet et al., 2021; Braak, 1972). This special case of the ERC has been resolved differently by neuroanatomical laboratories with some staying closer to conventional cortical nomenclature than others (see Table S1 for an overview; Behuet et al., 2021; Braak & Braak, 1991; Insausti et al., 1995). Between the cell-free layers lies a distinct layer of large, darkly stained pyramidal neurons (Braak & Braak, 1985; Insausti et al., 2017;

TABLE 3 Key features of the MTL cortex subregions.

	ERC	Perirhinal	Ectorhinal	PHC
Brodmann area	28, 34	35	36	-
Cortex type[a]	Periallocortex	Periallocortex and/or proisocortex	Proisocortex or isocortex	Periallocortex, proisocortex, and isocortex[b]
Location[c]	Crown of the parahippocampal and ambient gyri	Medial and/or lateral bank of the CS	CS and/or crown of the fusiform gyrus	Crown of the parahippocampal gyrus, medial bank of the CS
Seminal feature (see Figure 2)	- Layer II cell islands - *Lamina dissecans*[d] - Layer of large pyramidal cells adjacent to one or two *laminae dissecans*[d]	- Columnar organization of layers II and III - No *lamina dissecans*, but agranular and/or dysgranular layer IV	- Increasing granularity in layer IV - Gradual transition of layer VI to white matter	- Wide internal layers - Agrangular (medial) to granular (lateral) layer IV - Gradual transition between layers V and VI
Agreement[e]	High	Intermediate to high	Intermediate	Low to intermediate

Abbreviations: BA, Brodmann area; CS, collateral sulcus; ERC, entorhinal cortex; MTL cortex, parahippocampal gyrus; PHC, parahippocampal cortex.
[a]For the perirhinal and ectorhinal cortices there was disagreement on the type of cortex (indicated by "or").
[b]The seminal features below do not refer to the isocortex of the posterior PHC (Stenger et al., 2022).
[c]The gross anatomical location of subregions varies and is, among other things, dependent on the depth and ramification of the collateral sulcus (see Ding & Van Hoesen, 2010).
[d]Note that some neuroanatomists only refer to the external cell-free layer as *lamina dissecans*.
[e]See Table 4 for details.

Rose, 1927). Layers V and VI are close together and do not show sharp boundaries between each other and with the parahippocampal white matter (angular bundle) at anterior and intermediate levels, while the posterior ERC subfields show a sharp boundary with the white matter of the angular bundle (Insausti et al., 2017).

Annotations of the ERC along its longitudinal axis are exemplified in Figure 3a–c and their overlap in specimen 1 is visualized in Figure 4a (see Figure S2 for the other specimens). Generally, there was high agreement on border placement particularly in the mid-section of the ERC with slight variability shown at its anterior and posterior ends (Figures 3a,c and 4a). Indeed, neuroanatomists stated that the seminal cytoarchitectonic features of the ERC emerge only gradually at these anterior and posterior transitional sections, making annotations more difficult. An example of gradually developing layer II cell islands and *lamina dissecans* in the anterior ERC is shown in Figure 5a. In line with the previous neuroanatomical literature, the ERC was consistently bordered anteriorly by the rhinal/collateral sulci and sulcus semiannularis as well as superiorly by the periamygdaloid cortex, reflecting the substantial cytoarchitectonic differences between the six-layered ERC and the adjacent three-layered periamygdaloid cortex (Insausti et al., 2017). The medial border of the ERC was consistently placed adjacent to the hippocampal fissure, as well as the pre- or parasubiculum (Figures 3b,c and 4a; see also Ding & Van Hoesen, 2010; Insausti et al., 1995, 1998, 2017; Williams et al., 2023). As already depicted by Brodmann (1909), the ERC was encapsulated by perirhinal BA35 at its anterior, posterior, and lateral ends in all three specimens. Compared with the highly consistent superior and medial borders, there was some, albeit minor, variability in the placement of the ERC's lateral border with BA35, potentially due to the gradual transition of cytoarchitectonic features between the ERC and BA35 in this region. Figure 6b provides an example of slight variability in the placement of the border between ERC and BA35 in an anterior section, including a clarification of the different cytoarchitectonic features leading to this difference in border placement between neuroanatomists.

3.2.2 | Brodmann area 35

All neuroanatomists agreed that BA35, also called perirhinal cortex, is a heterogeneous structure located at the transition of periallocortex (i.e., ERC) to proisocortex. However, there was disagreement about the specific cortex type of BA35 as it was labeled dysgranular proisocortex by some, while others described both agranular periallocortical (e.g., BA35a) and dysgranular, proisocortical (e.g., BA35b) portions within BA35 (see Table 3, Table 4). Nevertheless, neuroanatomists agreed on several cytoarchitectonic features being characteristic to BA35. The pyramidal cells found in layers II and V are relatively large, though not as large as in the ERC. Layers II and III are organized in a distinct columnar fashion (Figure 2b). BA35 shows a unique layer III (by some neuroanatomists referred to as layer IIIu; Ding et al., 2009) which is formed by exceptionally large cells and lies internally to a typical layer III (see Figure 5b2; Augustinack, Huber, et al., 2013; Ding et al., 2009; Ding & Van Hoesen, 2010). At the medial border with the ERC, these features are expressed to form an oblique border, first appearing superficially, and extending into the midst of the cortex in a

TABLE 4 Agreement and disagreement among neuroanatomists about cytoarchitectonic features of the MTL cortex subregions.

		Disagreement			
Region	**Agreement**	**J. C. A.**	**O. K.**	**R. I.**	**S. L. D.**
ERC	**Periallocortex** L II: Clusters (or islands) of large stellate cells, interspersed with cell free areas L III: Wide layer with columnar organization of pyramidal cells L III & IV: *Lamina dissecans* formed by substrata of L III & IV (not both are equally present along the longitudinal extent of ERC) L V: Big, darkly stained pyramidal neurons L V & VI: No clear separation of layers (also with white matter) at anterior levels, clear boundary at posterior levels				
BA35	Wedge-like transition of lateral ERC to medial BA35 that extends from superficial cell layer to midst of the cortex L II & III: Relatively large cells, although not as large as in ERC; columnar organization L III: Presence of an oblique band of dark pyramidal cells[a] L V: Large pyramidal cells	**Periallocortex and proisocortex** L IV: Agranular (medial) to dysgranular (lateral) sections	**Periallocortex** L IV: Agranular	**Proisocortex** L IV: Agranular to dysgranular	**Periallocortex and proisocortex** L IV: Agranular (medial) to dysgranular (lateral) sections
BA36	L II: Small cells relative to ERC and BA35 L III-V: Higher cell density in lateral vs. medial portions L III: Small pyramidal cells relative to ERC and BA35 L V: Homogeneous with middle-sized to large pyramidal cells L VI: Fluent transition with white matter	**Isocortex** L IV: Granular	**Proisocortex** L III: Sublamination of L III into L IIIa-c (becomes clearer laterally) L IV: Dysgranular L V: Higher cell density in the lateral extensions	**Proisocortex** L IV: Dysgranular	**Isocortex** L IV: Granular
PHC	**Periallocortex transitioning to proisocortex** *TH/medial PHC*[b] **Periallocortex** L II: Can be patchy L II & III: Soft transition; superficial cells in L III are similar to LII L IV: Agranular L V: Thinner compared to TF, highly developed with large cells L V-VI: Soft transition but smaller and more densely packed cells in L VI; higher cell density than BA35 *TF/TL/TFm/lateral PHC*[c] **Proisocortex** L II: Thicker than TH/medial PHC L III: Higher cell density than BA36 L IV: Dysgranular L V: Highly developed with large cells L V-VI: Soft transition but more pronounced than in medial PHC	Annotated: *TH & TF* *TF* L III: Homogeneous; soft transition to L IV	Annotated: *PHC, Ph1-3* *Lateral PHC* L III: Sublamination of L III into L IIIa-c; L IIIa: contains small and densely packed cells; L IIIb has least cell density and relatively small cells; L IIIc contains middle-sized cells L IV: Soft transition to L V *Ph1-3* **Isocortex** For details see Stenger et al. (2022)	Annotated: *TH & TF* *TF* L III: Less columnarity than isocortex L IV: Thickens caudally	Annotated: *TH & TL/TFm* *TL/TFm (medial)* L IV: Soft transition to L V

Abbreviations: BA, Brodmann area; ERC, entorhinal cortex; L, layer; PHC, parahippocampal cortex.

[a]Note that some but not all neuroanatomists refer to this layer as IIIu.

[b]Medial PHC was used by O.K. and TH by the other neuroanatomists.

[c]TF can be divided into a medial and lateral part (TFm and TFl). TL is synonymous with TFm. TF was annotated by J.C.A. and R.I. TL/TFm was annotated by S.L. D. O.K. referred to this region as lateral PHC.

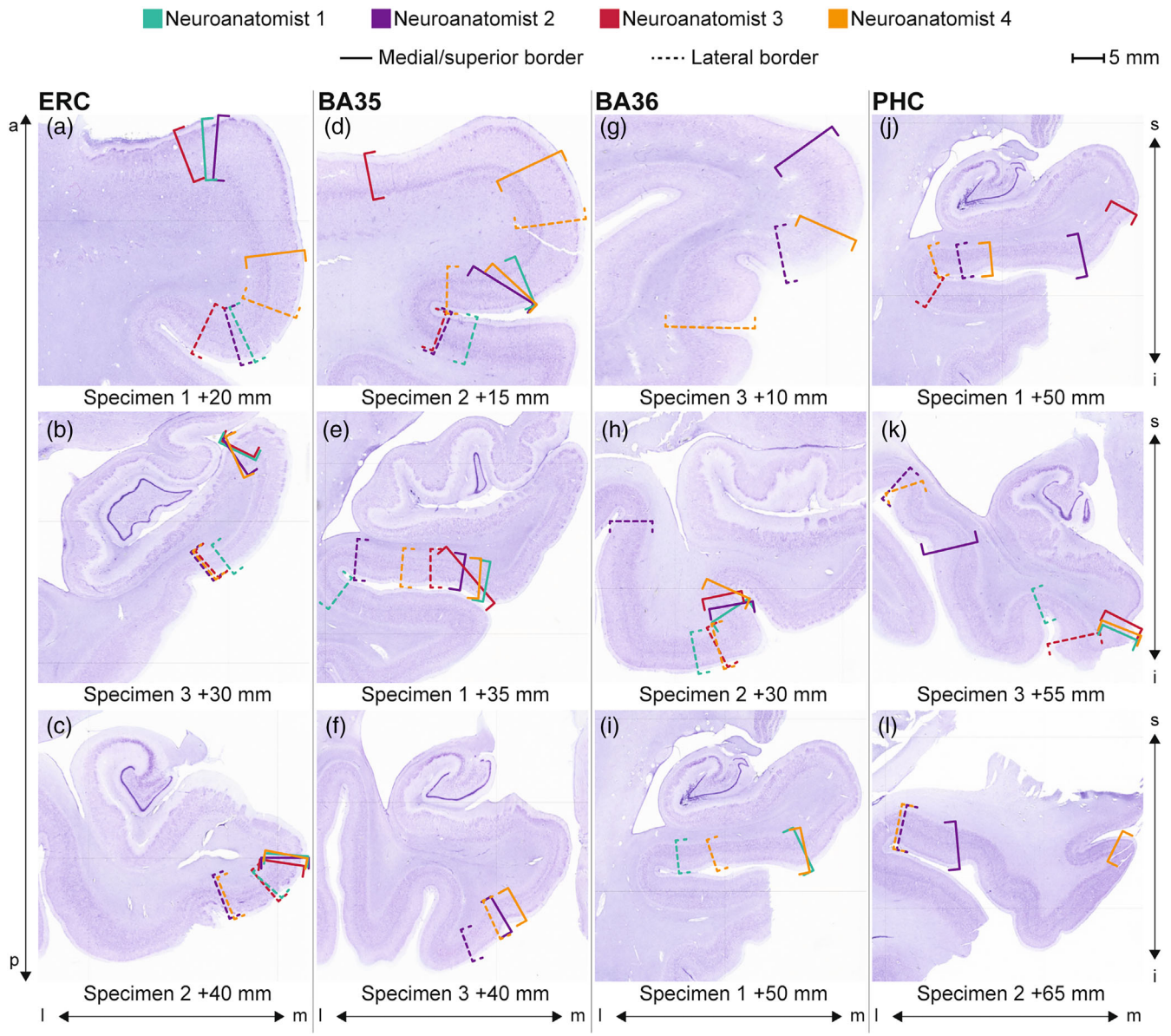

FIGURE 3 Annotations performed by the neuroanatomists for the anterior, mid-section, and posterior parts of four subregions of the MTL cortex. Millimeters indicate distance from the temporal pole. Sections were chosen to reflect the varying overlap of annotations across specimens and gross anatomical locations within the MTL cortex. a, anterior; BA, Brodmann area; ERC, entorhinal cortex; i, inferior; l, lateral; m, medial; p, posterior; PHC, parahippocampal cortex; s, superior.

lateral direction. Layer IIIu is difficult to distinguish from typical layer III using Nissl-staining, especially for non-experts (Figure 5b; Ding & Van Hoesen, 2010). However, as the pyramidal cells in layer IIIu are affected early by Alzheimer's disease-related neurofibrillary tau tangles (Braak & Braak, 1985; Ding & Van Hoesen, 2010), tau staining impressively revealed the unique, wedge-like shape of BA35's medial border in specimen 2 (Figure 5b1). BA35 closely corresponds to Braak's transentorhinal region (Braak & Braak, 1985). While for some neuroanatomists these terms are synonymous and refer to the same region, others stated that only the medial portions of their BA35 annotations (e.g., BA35a) can be referred to as transentorhinal cortex.

Across annotations, BA35 borders BA36 anterolaterally and PHC posterolaterally. Like the ERC, annotations in midsections of BA35 exhibited higher agreement among neuroanatomists (Figures 3e,f and 4, Figure S2), compared with anterior (Figure 3d) or posterior transitional sections. Figures 3 and 4 also show that, compared with annotations of the ERC, there was more variation among annotations in the medial-lateral dimension (see also Figure S2). Specifically, the lateral border of BA35 with BA36 varied among neuroanatomists. This was likely driven by the neuroanatomists' differing cytoarchitectonic definitions of BA35 with regards to layer IV granularity and cortex type (Table 4) and more importantly, by the gradual expression of layer IV granule cells when moving laterally (Figure 5b). Figure 6a

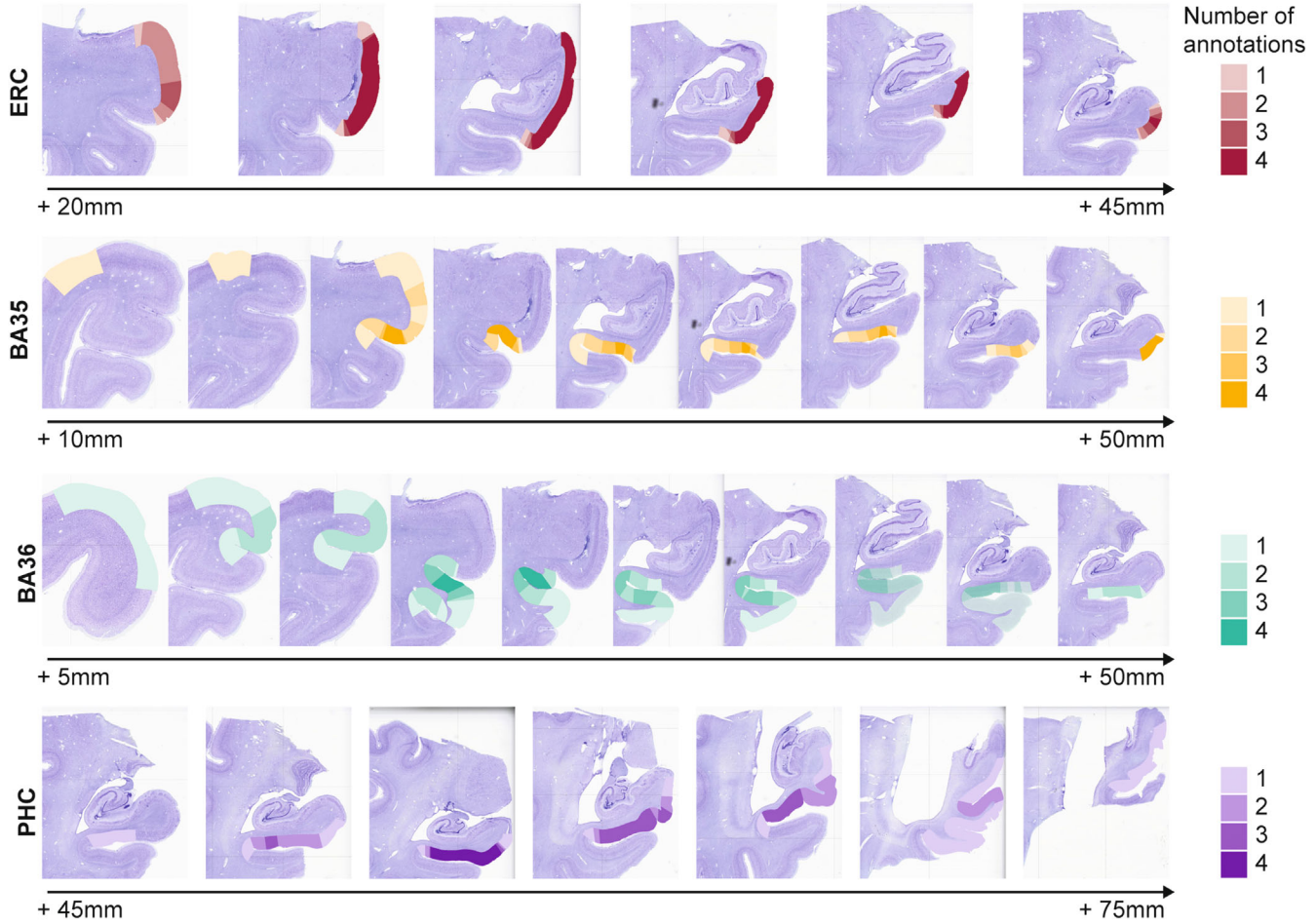

FIGURE 4 Overview of annotations of all four MTL cortex subregions in specimen 1 visualizing the overlap among neuroanatomists. Note the lower agreement (i.e., lighter colors) on transitional slices compared with higher agreement (i.e., darker colors) in midsections. The analogous visualization of annotations in specimens 2 and 3 can be found in Figure S2. Millimeters indicate distance from the temporal pole. BA, Brodmann area; ERC, entorhinal cortex; PHC, parahippocampal cortex.

provides an exemplary slice visualizing the differing annotations that resulted from these diverging definitions. Meanwhile, the medial border with the ERC had high agreement with minor variability (Figures 3d and 4), representing the large consensus on the cytoarchitectonic features of BA35 and the ERC in this region (i.e., cell islands in layer II of the ERC vs. large layer II/III cells arranged in columns in BA35).

3.2.3 | Brodmann area 36

BA36 was referred to as ectorhinal cortex by the neuroanatomists. Like BA35, neuroanatomists disagreed on the cortex type and thereby the extent of the layer IV granularity for BA36. While two neuroanatomists denoted BA36 as dysgranular proisocortex, others considered it a fully granular isocortical structure. The neuroanatomists agreed that layers II and III have smaller cells relative to the ERC and BA35, layer V is homogenous with middle to large pyramidal cells, and layer VI fluently transitions into white matter (Figure 2c).

BA36 borders other regions of the temporopolar cortex anteriorly and PHC as well as the peristriate cortex/BA19 posteriorly. Higher disagreement among neuroanatomists could be observed in these anterior and posterior transitional regions as opposed to the midsection of BA36 (Figures 3g–i and 4, Figure S2). Among all described structures, the annotations of BA36 exhibited the highest degree of disagreement in the medial-lateral dimension. The lateral border with BA20 varied profoundly. While three neuroanatomists included the lateral bank of the collateral sulcus (i.e., corresponding to Bordmann's original mapping of BA36), the annotations of one neuroanatomist additionally spanned the entire fusiform gyrus and medial bank of the occipitotemporal sulcus (i.e., also including some of BA20 on Brodmann's map or area TF as defined by von Economo and Koskinas; Figures 3h and 4). Similar to the border of BA35 with BA36, disagreements on the lateral border of BA36 with BA20 were at least partially caused by the gradual changes in granularity, which is susceptible to individual interpretation, along the medial–lateral axis (Figure 5b) and the neuroanatomists' different definitions of BA36 as either a proisocortical or isocortical structure (Table 4, see Figure 6a for how diverging definitions can lead

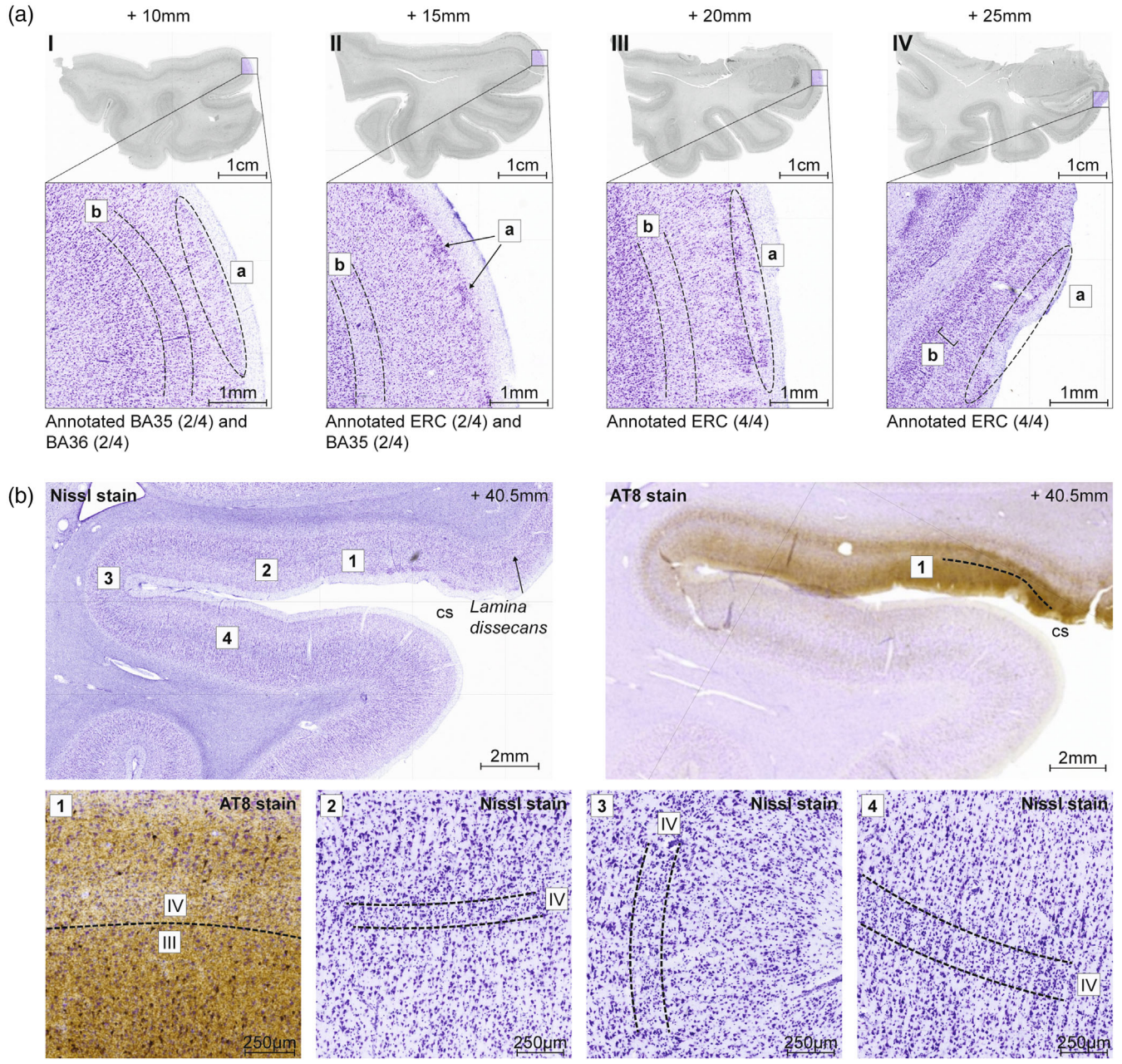

FIGURE 5 Gradual transition of cytoarchitectonic features in the MTL cortex. Panel (a) shows the gradual transition of the seminal cytoarchitectonic features of the ERC in an anterior-to-posterior direction in the anterior MTL cortex in specimen 2 (a-I to a-IV). Layer II cell islands are increasingly expressed moving posteriorly (a in a-I to a-IV). At the anterior level (b in a-I), layer IV comprises granule cells. In a-II and a-III cell-free sublaminae (*laminae dissecans*) can be identified. Two *laminae dissecans* are visible in the very posterior slice (b in a-IV). Note that some neuroanatomists only refer to the external cell-free sublamina as *lamina dissecans*. The annotations of the respective section are indicated below each slice. Panel (b) shows the gradual change from *lamina dissecans* (periallocortex) to a fully expressed granular layer IV in the medial-to-lateral direction along the collateral sulcus (cs) in specimen 1 (left slice). AT8 staining in panel (b) (right slice) exemplifies the wedge-like appearance of layer III (medial dotted line), made up of uniquely large pyramidal cells (referred to as layer IIIu by some neuroanatomists), which is characteristic for BA35. Panel (b1) shows a magnified image of the unique layer III in medial BA35 using AT8 staining. Panels (b2–4) indicate the increasing thickness, cell density, and organization of layer IV moving laterally along the collateral sulcus. Neuroanatomists annotated neighboring sections 0.5 mm anterior to the slices displayed in (b) as slices with both AT8 staining and Nissl staining-based annotations were unavailable according to the study protocol. Neuroanatomists annotated the section neighboring (b2) BA35 (2/4) and BA36 (2/4), the section neighboring (b3) BA36 (3/4) and transition from BA35 to BA36 (1/4), and the section neighboring (b4) BA36 (3/4) and non-MTL cortex (1/4). Millimeters indicate distance from the temporal pole. BA, Brodmann area; ERC, entorhinal cortex.

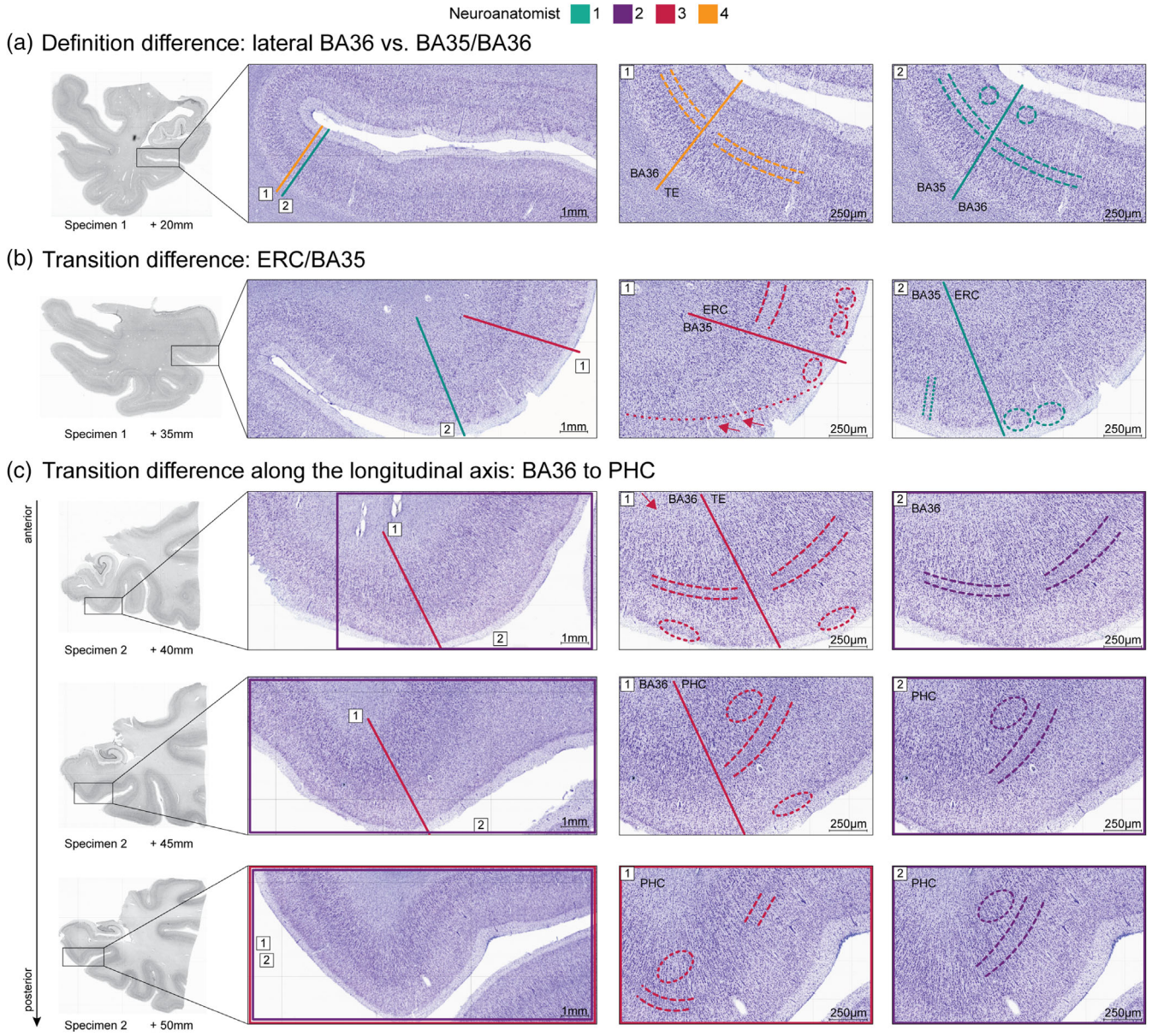

FIGURE 6 Examples of differences in delineations of the neuroanatomists in border regions of the MTL cortex. Panel (a) shows differing border placement due to disagreement in cytoarchitectonic definitions of BA35 and BA36. In (a1), the neuroanatomist annotated the lateral border of BA36 with region TE due to a change in granularity in layer IV (dashed lines). In the medial portion of this section (BA36), layer IV is present but not as prominent as in the lateral (region TE). In (a2), the neuroanatomist annotated a similarly positioned border but for regions BA35 and BA36. They also described a change in organization of layer IV granular cells (dashed lines). Moreover, smaller layer II cells in BA35 than in BA36 (circled) were indicated. Panel (b) shows a slightly different border placement in a transitional section between ERC and BA35. In (b1), the neuroananatomist identified a wedge-like transition between the two cortices (dotted line), with gradually emerging layer IIIu-cells (marked by arrows). Layer II cells (circled) are larger in ERC than in BA35 and the *lamina dissecans* is present only in ERC (dashed lines). In (b2), the neuroanatomist also identified cell clusters in layer II of the ERC. In BA35 (circled), cells in layers II and III are organized in elongated columns (dashed lines). Panel (c) shows differing border placement along the longitudinal axis of BA36 and PHC in an anterior to posterior fashion. In (c1), the neuroanatomist distinguishes BA36 and region TE on the most anterior slice. Here, BA36 is characterized by a gradual transition of gray into white matter (arrow) and a thinner layer IV (dashed lines) than found in region TE. Density of layer II cells is higher in region TE than in BA36 (circled). This portion posteriorly borders with PHC, with characteristic small cells and high cell packing density (circled) as well as a better-developed layer IV compared to BA36 (dashed lines). One section further posterior, only PHC is annotated due to a dysgranular layer IV (dashed lines), which is less developed than in region TE, and has a higher cell density than BA36 (circled). In (c2), another neuroanatomist annotated the whole anterior-most section as BA36, due to an absent layer IIIu and smaller layer IV cells (dashed lines) compared to BA35. The next section, moving one slice posterior, was annotated PHC as layer IV is well-developed (dashed lines) and smaller layer V and VI cells than found in BA36 (circled). In the adjacent posterior slice, PHC was annotated based on the same criteria. BA, Brodmann area; ERC, entorhinal cortex; PHC, parahippocampal cortex.

to differing annotations). Further, one neuroanatomist stated that their placement of the lateral BA36 border was guided by the position of the fundus of the occipitotemporal sulcus.

3.2.4 | Parahippocampal cortex

The PHC is another highly heterogeneous MTL subregion that spans periallocortical and proisocortical portions. In fact, one neuroanatomist stated that PHC even includes granular isocortex at its lateral end. Importantly, the neuroanatomists agreed that parcellation based on granularity is more difficult in the PHC than in more anterior subregions of the MTL cortex. Analogous to more anterior parts of the MTL cortex comprising the ERC and BA35, the medial bank of the collateral sulcus exhibits higher cytoarchitectonic heterogeneity at the level of the PHC. Neuroanatomists used various cytoarchitectonic definitions of the PHC which led to substantial differences in annotations, especially in their posterolateral extent (Table 4). In line with many of the previously proposed parcellations of the PHC in nonhuman primates (Blatt & Rosene, 1998; Ding & Van Hoesen, 2010; Suzuki & Amaral, 2003; Tranel et al., 1988) and in humans (Bailey & von Bonin, 1951; von Economo & Koskinas, 1925), its medial portion was referred to as region TH by two of the neuroanatomists. Here, layer II and III cell bodies are rather small, layer IV is absent (agranular), and layers V and VI are homogeneously transitioning into one another (Figure 2d; note that here an incipient granule cell layer may be visible). Relative to BA35, the medial PHC has a higher cell density and wider internal layers (Figure 2d). Neuroanatomists who distinguished the PHC subregions divided the lateral PHC into either as TFm (medial) and TFl (lateral; as introduced in the Macaca fascicularis monkey by Suzuki & Amaral, 2003) or as TL (as described also in primates by Blatt & Rosene, 1998). Here, layer II is thicker than in the medial PHC, layer III exhibits high columnar organization, weakly organized granule cells form an incipient dysgranular layer IV, and the transition of layers V and VI is gradual and almost imperceptible (Figure 2e). One neuroanatomist additionally included more posterior regions (referred to as Ph1-3) in their annotations of the PHC (see Figure 4 and Figure S2). These isocortical regions were characterized by a fully organized granular layer IV, though its prominence varied among the single subregions (see Appendix S1 for more details on regions Ph1-3).

All neuroanatomists placed the PHC posterior to BA35, lateral to the parasubiculum or transsubiculum, and medial to the fundus of the posterior collateral sulcus extending as far as the posterior tip of the corpus callosum. Similar to the medial ERC border, the medial PHC border was annotated with high consistency in midsections (i.e., at the level of the hippocampal body; Figure 3). Figures 3, 4, and 6c additionally show the high disagreement in border placement in the posterior and lateral extent of the PHC. Note that if the isocortical Ph subregion is not considered, which has been proposed to be part of the human PHC only recently (Stenger et al., 2022) and was annotated only by one neuroanatomist, the agreement among neuroanatomists on the PHC would be higher.

4 | DISCUSSION

In this study, we give an overview of the cytoarchitectonic definitions of MTL cortex subregions (ERC, BA35, BA36, and PHC), aiming to examine and understand the underlying reasons for overlapping and diverging annotations made by four independent neuroanatomists. We find highest agreement of border placement for the ERC and lowest agreement for the PHC, while annotations of BA35 and BA36 show intermediate overlap. Importantly, the degree of agreement on definitions of cytoarchitectonic features does not necessarily correspond to agreement in border placement, since even structures with substantial agreement in described seminal features could show highly diverging annotations and vice versa. This partial mismatch of annotations and formal cytoarchitectonic definitions is due to additional factors influencing inter- and intra-rater reliability of neuroanatomical annotations as discussed below. Despite these differences, an extensive overlap of annotations among neuroanatomists is observed. Overall, the presented dataset of histological annotations uniquely informs in vivo neuroimaging research.

4.1 | Various factors influence the differences among neuroanatomists' annotations

Based on the present results, we identify several factors which appear to influence the (dis-)agreement in annotations among neuroanatomists, underlining the complexity of annotating MTL cortex subregions.

First, disagreements are partially caused by varying definitions of features of MTL cortex subregions, as discussed above. These differences may partially stem from different traditions, backgrounds, and research foci of the neuroanatomists. For example, neuroanatomical schools may put particular emphasis on the subregions' structural or functional connectivity, receptor architecture, or chemoarchitecture. Subsequently, this may lead to different perceptions and interpretations of histological information. For instance, we observed that while neuroanatomists agreed on the formal definition of different types of cortex, they did not allocate these to the same MTL cortex subregions. An example is proisocortex and the disagreement on whether this includes only BA35 or both BA35 and BA36. In several cases, the proisocortical BA35b of one and the proisocortical BA36 of another neuroanatomist were delineated almost identically. Additional variability may be introduced by the fact that neuroanatomical schools differ in their use of gross anatomical information for their annotations. This ranges from explicitly considering gross anatomy for border placement, using this information for orientation purposes, to dismissing gross anatomical landmarks and solely relying on histological information.

Second, we observed that annotations diverged in transitional areas between structures. Transition sharpness clearly differs within the MTL cortex, influencing the overlap of annotations. For example, the transition between the ERC and hippocampal structures is relatively salient, leaving little room for uncertainty and leading to higher agreement among neuroanatomists. Meanwhile, there are other transitional areas, such as the area between BA35 and BA36, where the

features of multiple subregions are expressed. As the neuroanatomists may weigh these features differently, they may come to different conclusions and place the respective border at different locations. This ambiguity does not only impact inter-rater reliability; neuroanatomists also highlighted that intra-rater reliability (i.e., one neuroanatomist rating the same specimen twice) would likely be lower in these transitional areas.

Third, the neuroanatomists' certainty and, in turn, the agreement of annotations, is influenced by aspects related to the sectioning procedure chosen in this study. The difficulty of annotating transitional zones may increase when borders between structures do not run strictly parallel or perpendicular to the provided sections. Even when using a consistent plane of sectioning (i.e., orthogonal to anterior commissure–posterior commissure (AC–PC) line) the irregular surface of the MTL—alongside the obliquity of sulci and other gross anatomical landmarks—can add complexity and ambiguity to the interpretation of boundaries. In such cases, it is possible that sections of one subregion are interrupted by portions of other types of cortices (e.g., appearance of olfactory cortex surrounded by the ERC). In the present dataset, slices were cut perpendicular to the long axis of the hippocampus to aid the translation to thick-sliced in vivo MRI. For most neuroanatomists this is different from the common coronal sections cut perpendicular to the AC–PC line direction, which may have decreased certainty in border placement as well. While we observed disagreement of annotations in transitional zones in all directions, transitions between sections (i.e., along the longitudinal axis) appear to cause more uncertainty than those within sections (i.e., on the medial to lateral axis). This may be because continuous information is only available within histological slices, making it more difficult to perceive differences between MTL cortical regions along the longitudinal axis. It is likely that this effect was exacerbated since three neuroanatomists were initially provided with histological slices spaced 5 mm apart, making subtle changes in cytoarchitectonic features more difficult to detect.

A fourth influencing factor pointed out by the neuroanatomists is the historical focus (or lack of it) on some subregions over the others. The PHC, for example, is historically understudied in its seminal cytoarchitectonic features, connectivity, and borders with other structures. Most research on the PHC has been done in non-human primates (e.g., Blaizot et al., 2004; Suzuki & Amaral, 1994; von Bonin & Bailey, 1947) and translational studies have only recently emerged (e.g., Stenger et al., 2022). Thus, less information is available on the cytoarchitectonic features of the human PHC (Bailey & von Bonin, 1951; Ding et al., 2016; Ding & Van Hoesen, 2010; Mai et al., 2015; von Economo & Koskinas, 1925), resulting in lower agreement in parcellations.

Fifth, neuroanatomists pointed out that annotating at sulcal fundi is generally challenging as most cellular layers are compressed (see e.g., von Economo & Koskinas, 1929). This factor is relevant to the annotation of the border between BA35 and BA36 as well as the lateral border of the PHC as both are often located in proximity to the fundus of the collateral sulcus.

Finally, neuroanatomists indicated that their uncertainties were amplified in the third specimen due to severe neurodegeneration of the MTL cortex. Cell loss that particularly affects certain neuronal populations and cortical layers distorts the overall cytoarchitectonic appearance of the cortex, potentially posing a significant challenge for neuroanatomical annotations. The uncertainty regarding the exact border locations may have contributed to higher disagreement across all annotated subregions in this specific specimen.

Performing annotations as presented in this study requires neuroanatomists to integrate various features of the provided specimen. Considering the aforementioned challenges leading to subjective uncertainty and disagreement among neuroanatomical schools, the present delineations of MTL cortex subregions exhibit impressively high overlap, particularly in the ERC and BA35. Importantly, we observed overlap among labels for regions with similar cytoarchitectonic definitions despite discrepant terminology (e.g., proisocortical BA35b and proisocortical BA36, region TH and medial PHC). While this is a promising finding that suggests that converging cytoarchitectonic definitions can indeed translate to overlapping annotations, we would like to emphasize the importance of harmonized terminology. After all, correspondence and collaboration among researchers relies on efficient communication that requires a common language to avoid misunderstandings and inaccuracies.

While helping to explain why annotations differ among neuroanatomists, this knowledge cannot bridge the current gap that hinders a consensus on histologically-defined definitions of subregions in the human MTL cortex. Such a consensus among neuroanatomists is highly desirable and will benefit the research community. The information gained from this study, nonetheless, can help advance and inform neuroimaging research of the MTL. This includes providing insights, for example, for the efforts of the Hippocampal Subfields Group on the development of a histologically-informed harmonized segmentation protocol for the MTL cortex or for findings localized in the MTL cortex in functional MRI research.

4.2 | Implications for in vivo neuroimaging research

For human neuroimaging research, the precise and harmonized understanding of neuroanatomical entities ranging from small brain regions (such as MTL cortex subregions) to whole functional brain networks is crucial for synergistic work within and across research fields. The validity of labels applied in neuroimaging studies stems from a histologically-defined ground truth and is key for integration and comparison of findings across a broader literature and for developing theories of brain structure, function, and pathology. An example for such collaborative processes is the investigation of the complex mechanisms underlying cognitive decline in neurodegenerative diseases such as Alzheimer's disease. It requires the integration of insights from a wide range of research fields, ranging from in vivo functional MRI studies of functional specialization and/or gradients within the MTL, in vivo positron emission tomography studies to quantify pathology burden at different disease stages, to ex vivo structural MRI to explore the earliest neurodegenerative effects of

Alzheimer's disease pathology. Combining this multitude of research foci, modalities, and backgrounds requires a common language and harmonized neuroanatomical definitions. Keeping the aforementioned limitations of histological annotations in mind (e.g., reduced reliability due to cell loss), the presented overview of cytoarchitectonic features of MTL cortex subregions from four different neuroanatomical laboratories aids in further advancing human neuroimaging research in all of its applications and modalities.

The need for harmonization in neuroimaging is demonstrated in the variety of MRI segmentation protocols dedicated to the MTL (Berron et al., 2017; Feczko et al., 2009; Insausti et al., 1998; Kivisaari et al., 2020; Olsen et al., 2013; Pruessner et al., 2002; Wisse et al., 2017; Xie et al., 2019; Yushkevich, Pluta, et al., 2015). Our study shows that while there is notable agreement among neuroanatomists in the cytoarchitectonic features referenced, there is currently no single neuroanatomical ground truth for the delineation of MTL cortex subregions on histological slices. As segmentation protocols for in vivo MRI commonly rely on a single neuroanatomical school, profound differences are inevitable. Consequently, in vivo neuroimaging studies of the MTL often lack comparability, negatively impacting their generalizability and usefulness for meta-analyses. To resolve this issue, harmonized definitions of MTL cortex subregions are needed for neuroimaging. Our present study sets an important foundation for this effort by providing an overview of how MTL cortex subregions are defined and delineated by different neuroanatomical schools. Our observations of highly overlapping annotations in certain regions are especially encouraging for neuroimaging research that operates at resolutions that make many of the observed differences negligible. The Hippocampal Subfields Group is currently working towards establishing a harmonized segmentation protocol of the MTL cortex based on the presented findings.

4.3 | Strengths and limitations

A major strength of the present study is the integration of input from four leading expert neuroanatomists in the field, forming a first-of-its-kind annotated dataset of MTL cortex subregions in three histological specimens representing varying demographic backgrounds and anatomical variability. Yet, the limitations of the study must also be considered.

First, no quantitative investigation of the differences in annotations was performed. Due to the numerous factors that influence the annotations of the neuroanatomists, we believe that it is not warranted to assess the differences in annotations quantitatively. Furthermore, focusing on quantitative measures of inter-rater agreement may lead to false conclusions and obscure the fine-grained picture that we are describing in this study. Instead, we show that considering the complexity of this work is of utmost importance when investigating the fine-grained neuroanatomy of the MTL cortex.

Second, the generalizability of our results is limited as the presented information is based on a small sample of three specimens. It has been reported that the location of MTL cortex subregions varies with collateral sulcus depth and ramification (Ding & Van Hoesen, 2010; Insausti et al., 1998). Although we included samples with different collateral sulcus depths and ramifications to account for this to some extent, a sample size of three specimens is clearly insufficient to fully characterize the role of anatomical variants in MTL subregion delineations. Unfortunately, because of the time and effort required (~9 h per specimen) to generate a dataset comprising the entirety of macroscopic MTL cortex phenotypes it was not possible to perform the current comparison between neuroanatomical schools in a larger sample. Nevertheless, we believe the characterization of the three specimens in this study still provide valuable insights.

Third, generalizability may also be impaired as we included "only" four neuroanatomists. There may be experts in the field who rely on neuroanatomical procedures that were not detailed here (e.g., intracellular filling). However, once again, we note that those techniques would be in principle limited to a small amount of the volume of the whole MTL cortex. Still, to our knowledge, the shown synthesis of neuroanatomical expertise goes beyond the efforts of other studies in the field, substantially improving upon the diverging opinions.

Finally, Nissl-stained sections provide optimal cytoarchitectural boundaries (Swanson, 2003), making them reliable for performing mass parcellations (Williams et al., 2023). Meanwhile, immunochemical markers may be used in combination with Nissl-stained sections to annotate complex and heterogeneous regions like the MTL cortex (e.g., Ding et al., 2009; Ding & Van Hoesen, 2010). The fact that we utilized Nissl-stained sections may have negatively affected the certainty of some neuroanatomists. However, the additional use of complementary techniques would not disambiguate the borders for all neuroanatomists. The time and effort required to implement such techniques, thus, do not justify their use.

5 | CONCLUSION

In summary, our detailed histological investigation shows that, aside from some disagreements, there is high overlap of definitions and delineations of subregions in the MTL cortex. These findings not only advance our neuroanatomical understanding of this important brain region but also provide a rich foundation for all neuroimaging research investigating the human MTL. Moreover, the in-depth understanding of disagreements among neuroanatomists likely translates to other brain regions, where similar degrees of disagreement are potentially present. This is evident for the hippocampus, where differences in annotations were observed among neuroanatomists (Olsen et al., 2019) and for neocortical regions as evidenced by different automated segmentations for in vivo MRI (Huizinga et al., 2021; Gomez-Ramirez et al., 2022), potentially reflecting underlying differences in cytoarchitectonic definitions as well.

AFFILIATIONS

[1]Clinical Memory Research Unit, Department of Clinical Sciences Malmö, Lund University, Lund, Sweden

[2]German Center for Neurodegenerative Diseases (DZNE), Magdeburg, Germany

[3]Department of Neurobiology and Behavior, University of California, Irvine, Irvine, California, USA

[4]INSERM UMR-S U1237, PhIND "Physiopathology and Imaging of Neurological Disorders", Institut Blood and Brain @ Caen-Normandie, Caen-Normandie University, GIP Cyceron, France

[5]Royal Holloway, University of London, Egham, UK
[6]University of Toronto, Toronto, Ontario, Canada
[7]Rotman Research Institute, Toronto, Ontario, Canada
[8]Department of Psychological and Brain Sciences, Johns Hopkins University, Baltimore, Maryland, USA
[9]Department of Psychology, Stanford University, Stanford, California, USA
[10]Department of Psychiatry and Behavioral Sciences, Johns Hopkins University, Baltimore, Maryland, USA
[11]Institute of Gerontology, Wayne State University, Detroit, Michigan, USA
[12]School of Psychology, University of Sydney, Sydney, Australia
[13]Department of Psychology, Wayne State University, Detroit, Michigan, USA
[14]Memory and Aging Center, Department of Neurology, Weill Institute for Neurosciences, University of California, San Francisco, California, USA
[15]The Ohio State University, Columbus, Ohio, USA
[16]Department of Pharmacology, University of North Carolina at Chapel Hill, Chapel Hill, North Carolina, USA
[17]Human Neuroanatomy Laboratory, University of Castilla-La Mancha, Albacete, Spain
[18]University of Pennsylvania, Philadelphia, Pennsylvania, USA
[19]Institute of Neuroscience and Medicine (INM-1), Research Center Jülich, Jülich, Germany
[20]C. & O. Vogt Institute for Brain Research, Medical Faculty, University Hospital Düsseldorf, Heinrich-Heine-University, Düsseldorf, Germany
[21]Massachusetts General Hospital, Boston, Massachusetts, USA
[22]Allen Institute for Brain Science, Seattle, Washington, USA
[23]Department of Diagnostic Radiology, Lund University, Lund, Sweden

ACKNOWLEDGMENTS

We would like to acknowledge the donors and their family members for making this work possible. Special thanks go to the Marcus Wallenberg foundation for international scientific collaboration (2020.0004) and the Wenner-Gren foundation (ESh2020-002) for their generous support. This work was supported by NIH grants R01-AG070592, P01AG066597 and P30AG072979. Additionally, this study was supported by MultiPark - A Strategic Research Area at Lund University and by the Intramural UCLM grant GRIN 31097.

J.N.A. was supported by the National Institute on Aging NRSA (F32AG074621). C.J.H. was supported by funding from the Biotechnology and Biological Sciences Research Council (BB/V010549/1). R.K.O. was supported by funding from the Canadian Institutes of Health Research (CIHR PJT162292) and the Alzheimer Society of Canada. T.T.T. was supported by the National Institute on Aging NRSA (F32AG071263), and the Alzheimer's Association (AARFD-21-852597). P.Y. was supported by NIH grants P30 AG072979 and RF1 AG056014. O.K. and K.A. received funding from the European Union's Horizon 2020 Research and Innovation Programme under the Specific Grant Agreement No. 945539 (Human Brain Project SGA3). J.C.A. was supported by NIH grants R01AG057672 and RF1AG072056. R.I. was supported by the Intramural UCLM grant GRIN 31097.

CONFLICT OF INTEREST STATEMENT

The authors of this manuscript have nothing to declare.

DATA AVAILABILITY STATEMENT

Data can be shared upon completion of the harmonized protocol for the MTL cortex in a subsequent manuscript.

ORCID

Anika Wuestefeld https://orcid.org/0000-0003-1779-3388
Hannah Baumeister https://orcid.org/0000-0001-5503-6308
Jenna N. Adams https://orcid.org/0000-0002-6702-3851
Robin de Flores https://orcid.org/0000-0003-3953-3392
Carl J. Hodgetts https://orcid.org/0000-0002-0339-2447
Negar Mazloum-Farzaghi https://orcid.org/0000-0002-8149-6858
Rosanna K. Olsen https://orcid.org/0000-0002-2918-4152
Tammy T. Tran https://orcid.org/0000-0001-7728-9621
Arnold Bakker https://orcid.org/0000-0003-0417-641X
Kelsey L. Canada https://orcid.org/0000-0002-0366-1555
Eunice Chung https://orcid.org/0000-0002-8386-9427
María del Mar Arroyo-Jiménez https://orcid.org/0000-0002-8390-5352
Emilio Artacho-Pérula https://orcid.org/0000-0002-2201-576X
David J. Irwin https://orcid.org/0000-0002-5599-5098
Edward B. Lee https://orcid.org/0000-0002-4589-1180
Sydney Lim https://orcid.org/0000-0002-5359-4661
Monica Munoz Lopez https://orcid.org/0000-0002-5530-2394
Carlos de la Rosa Prieto https://orcid.org/0000-0003-1644-1735
Paul Yushkevich https://orcid.org/0000-0001-8543-4016
David Berron https://orcid.org/0000-0003-1558-1883
Laura E. M. Wisse https://orcid.org/0000-0001-7504-3943

REFERENCES

Augustinack, J. C., Huber, K. E., Stevens, A. A., Roy, M., Frosch, M. P., van der Kouwe, A. J. W., Wald, L. L., Van Leemput, K., McKee, A. C., & Fischl, B. (2013). Predicting the location of human perirhinal cortex, Brodmann's area 35, from MRI. *NeuroImage*, *64*, 32–42. https://doi.org/10.1016/j.neuroimage.2012.08.071

Augustinack, J. C., van der Kouwe, A. J. W., & Fischl, B. (2013). Medial temporal cortices in ex vivo magnetic resonance imaging. *Journal of Comparative Neurology*, *521*(18), 4177–4188. https://doi.org/10.1002/cne.23432

Bailey, P., & von Bonin, G. (1951). *The isocortex of man*. University of Illinois Press.

Bailey, P., von Bonin, G., & McCulloch, W. S. (1950). *The isocortex of the chimpanzee*. Univ. Illinois Press.

Behuet, S., Bludau, S., Kedo, O., Schiffer, C., Dickscheid, T., Brandstetter, A., Massicotte, P., Omidyeganeh, M., Evans, A., & Amunts, K. (2021). A high-resolution model of the human entorhinal cortex in the 'BigBrain' – Use case for machine learning and 3D analyses. In K. Amunts, L. Grandinetti, T. Lippert, & N. Petkov (Eds.), *Brain-inspired computing* (pp. 3–21). Springer International Publishing. https://doi.org/10.1007/978-3-030-82427-3_1

Berron, D., Vieweg, P., Hochkeppler, A., Pluta, J. B., Ding, S.-L., Maass, A., Luther, A., Xie, L., Das, S. R., Wolk, D. A., Wolbers, T., Yushkevich, P. A., Düzel, E., & Wisse, L. E. M. (2017). A protocol for manual segmentation of medial temporal lobe subregions in 7Tesla MRI. *NeuroImage: Clinical*, *15*, 466–482. https://doi.org/10.1016/j.nicl.2017.05.022

Berron, D., Vogel, J. W., Insel, P. S., Pereira, J. B., Xie, L., Wisse, L. E. M., Yushkevich, P. A., Palmqvist, S., Mattsson-Carlgren, N., Stomrud, E., Smith, R., Strandberg, O., & Hansson, O. (2021). Early stages of tau pathology and its associations with functional connectivity, atrophy and memory. *Brain*, *114*, 2771–2783. https://doi.org/10.1093/brain/awab114

Blaizot, X., Martinez-Marcos, A., Arroyo-Jimenez, M. d. M., Marcos, P., Artacho-Pérula, E., Muñoz, M., Chavoix, C., & Insausti, R. (2004). The parahippocampal gyrus in the baboon: Anatomical, cytoarchitectonic and magnetic resonance imaging (MRI) studies. *Cerebral Cortex*, *14*(3), 231–246. https://doi.org/10.1093/cercor/bhg123

Blatt, G. J., & Rosene, D. L. (1998). Organization of direct hippocampal efferent projections to the cerebral cortex of the rhesus monkey: Projections from CA1, prosubiculum, and subiculum to the temporal lobe. *Journal of Comparative Neurology*, *392*(1), 92–114. https://doi.org/10.1002/(SICI)1096-9861(19980302)392:1<92::AID-CNE7>3.0.CO;2-K

Braak, H. (1972). Zur Pigmentarchitektonik der Großhirnrinde des Menschen. *Zeitschrift für Zellforschung Und Mikroskopische Anatomie*, *127*(3), 407–438. https://doi.org/10.1007/BF00306883

Braak, H., & Braak, E. (1985). On areas of transition between entorhinal allocortex and temporal isocortex in the human brain. Normal morphology and lamina-specific pathology in Alzheimer's disease. *Acta Neuropathologica*, *68*(4), 325–332. https://doi.org/10.1007/BF00690836

Braak, H., & Braak, E. (1991). Neuropathological stageing of Alzheimer-related changes. *Acta Neuropathologica*, *82*(4), 239–259. https://doi.org/10.1007/BF00308809

Braak, H., & Braak, E. (1992). The human entorhinal cortex: Normal morphology and lamina-specific pathology in various diseases. *Neuroscience Research*, *15*(1), 6–31. https://doi.org/10.1016/0168-0102(92)90014-4

Braak, H., & Braak, E. (1995). Staging of alzheimer's disease-related neurofibrillary changes. *The Schmitt Symposium: The Cytoskeleton and Alzheimer's Disease*, *16*(3), 271–278. https://doi.org/10.1016/0197-4580(95)00021-6

Brodmann, K. (1909). *Vergleichende Lokalisationslehre der Grosshirnrinde in ihren Prinzipien dargestellt auf Grund des Zellenbaues*. Barth.

Ding, S.-L., Royall, J. J., Sunkin, S. M., Ng, L., Facer, B. A. C., Lesnar, P., Guillozet-Bongaarts, A., McMurray, B., Szafer, A., Dolbeare, T. A., Stevens, A., Tirrell, L., Benner, T., Caldejon, S., Dalley, R. A., Dee, N., Lau, C., Nyhus, J., Reding, M., … Lein, E. S. (2016). Comprehensive cellular-resolution atlas of the adult human brain. *Journal of Comparative Neurology*, *524*(16), 3127–3481. https://doi.org/10.1002/cne.24080

Ding, S.-L., & Van Hoesen, G. W. (2010). Borders, extent, and topography of human perirhinal cortex as revealed using multiple modern neuroanatomical and pathological markers. *Human Brain Mapping*, *31*(9), 1359–1379. https://doi.org/10.1002/hbm.20940

Ding, S.-L., Van Hoesen, G. W., Cassell, M. D., & Poremba, A. (2009). Parcellation of human temporal polar cortex: A combined analysis of multiple cytoarchitectonic, chemoarchitectonic and pathological markers. *The Journal of Comparative Neurology*, *514*(6), 595–623. https://doi.org/10.1002/cne.22053

Doan, T. P., Lagartos-Donate, M. J., Nilssen, E. S., Ohara, S., & Witter, M. P. (2019). Convergent projections from perirhinal and postrhinal cortices suggest a multisensory nature of lateral, but not medial, entorhinal cortex. *Cell Reports*, *29*(3), 617–627.e7. https://doi.org/10.1016/j.celrep.2019.09.005

Eichenbaum, H., Otto, T., & Cohen, N. J. (1994). Two functional components of the hippocampal memory system. *Behavioral and Brain Sciences*, *17*(3), 449–472. https://doi.org/10.1017/S0140525X00035391

Feczko, E., Augustinack, J. C., Fischl, B., & Dickerson, B. C. (2009). An MRI-based method for measuring volume, thickness and surface area of entorhinal, perirhinal, and posterior parahippocampal cortex. *Neurobiology of Aging*, *30*(3), 420–431. https://doi.org/10.1016/j.neurobiolaging.2007.07.023

Filimonoff, I. N. (1947). A rational subdivision of the cerebral cortex. *Archives of Neurology and Psychiatry*, *58*(3), 296–311. https://doi.org/10.1001/archneurpsyc.1947.02300320047002

Fischl, B., Stevens, A. A., Rajendran, N., Yeo, B. T. T., Greve, D. N., Van Leemput, K., Polimeni, J. R., Kakunoori, S., Buckner, R. L., Pacheco, J., Salat, D. H., Melcher, J., Frosch, M. P., Hyman, B. T., Grant, P. E., Rosen, B. R., van der Kouwe, A. J. W., Wiggins, G. C., Wald, L. L., & Augustinack, J. C. (2009). Predicting the location of entorhinal cortex from MRI. *NeuroImage*, *47*(1), 8–17. https://doi.org/10.1016/j.neuroimage.2009.04.033

Gomez-Ramirez, J., Quilis-Sancho, J., & Fernandez-Blazquez, M. A. (2022). A comparative analysis of MRI automated segmentation of subcortical brain volumes in a large dataset of elderly subjects. *Neuroinformatics*, *20*(1), 63–72. https://doi.org/10.1007/s12021-021-09520-z

Gottfried, J. A. (2010). Central mechanisms of odour object perception. *Nature Reviews Neuroscience*, *11*(9), 628–641. https://doi.org/10.1038/nrn2883

Hannula, D. E., & Duff, M. C. (Eds.). (2017). *The hippocampus from cells to systems*. Springer International Publishing. https://doi.org/10.1007/978-3-319-50406-3

Huizinga, W., Poot, D. H. J., Vinke, E. J., Wenzel, F., Bron, E. E., Toussaint, N., Ledig, C., Vrooman, H., Ikram, M. A., Niessen, W. J., Vernooij, M. W., & Klein, S. (2021). Differences between MR brain region segmentation methods: Impact on single-subject analysis. *Frontiers in Big Data*, *4*, 577164. https://doi.org/10.3389/fdata.2021.577164

Hyman, B. T., Phelps, C. H., Beach, T. G., Bigio, E. H., Cairns, N. J., Carrillo, M. C., Dickson, D. W., Duyckaerts, C., Frosch, M. P., Masliah, E., Mirra, S. S., Nelson, P. T., Schneider, J. A., Thal, D. R., Thies, B., Trojanowski, J. Q., Vinters, H. V., & Montine, T. J. (2012). National Institute on Aging–Alzheimer's Association guidelines for the neuropathologic assessment of Alzheimer's disease. *Alzheimer's & Dementia*, *8*(1), 1–13. https://doi.org/10.1016/j.jalz.2011.10.007

Iizuka, N., Masaoka, Y., Kubota, S., Sugiyama, H., Yoshida, M., Yoshikawa, A., Koiwa, N., Honma, M., Watanabe, K., Kamijo, S., Kamimura, S., Ida, M., Ono, K., & Izumizaki, M. (2021). Entorhinal cortex and parahippocampus volume reductions impact olfactory decline in aged subjects. *Brain and Behavior*, *11*(5), e02115. https://doi.org/10.1002/brb3.2115

Insausti, R., Amaral, D. G., & Cowan, W. M. (1987). The entorhinal cortex of the monkey: II. Cortical afferents. *Journal of Comparative Neurology*, *264*(3), 356–395. https://doi.org/10.1002/cne.902640306

Insausti, R., Córcoles-Parada, M., Ubero, M. M., Rodado, A., Insausti, A. M., & Muñoz-López, M. (2019). Cytoarchitectonic areas of the gyrus ambiens in the human brain. *Frontiers in Neuroanatomy*, *13*, 21. https://doi.org/10.3389/fnana.2019.00021

Insausti, R., Insausti, A. M., Muñoz López, M., Medina Lorenzo, I., Arroyo-Jiménez, M. d. M., Marcos Rabal, M. P., de la Rosa-Prieto, C., Delgado-González, J. C., Montón Etxeberria, J., Cebada-Sánchez, S., Raspeño-García, J. F., Iñiguez de Onzoño, M. M., Molina Romero, F. J., Benavides-Piccione, R., Tapia-González, S., Wisse, L. E. M., Ravikumar, S., Wolk, D. A., DeFelipe, J., … Artacho-Pérula, E. (2023). Ex vivo, in situ perfusion protocol for human brain fixation compatible with microscopy, MRI techniques, and anatomical studies. *Frontiers in Neuroanatomy*, *17*, 1149674. https://doi.org/10.3389/fnana.2023.1149674

Insausti, R., Juottonen, K., Soininen, H., Insausti, A. M., Partanen, K., Vainio, P., Laakso, M. P., & Pitkänen, A. (1998). MR volumetric analysis

of the human entorhinal, perirhinal, and temporopolar cortices. *American Journal of Neuroradiology*, *19*(4), 659–671.

Insausti, R., Muñoz-López, M., Insausti, A. M., & Artacho-Pérula, E. (2017). The human periallocortex: Layer pattern in presubiculum, parasubiculum and entorhinal cortex. A review. *Frontiers in Neuroanatomy*, *11*, 84. https://doi.org/10.3389/fnana.2017.00084

Insausti, R., Tuñón, T., Sobreviela, T., Insausti, A. M., & Gonzalo, L. M. (1995). The human entorhinal cortex: A cytoarchitectonic analysis. *Journal of Comparative Neurology*, *355*(2), 171–198. https://doi.org/10.1002/cne.903550203

Kivisaari, S. L., Probst, A., & Taylor, K. I. (2020). The perirhinal, entorhinal, and parahippocampal cortices and hippocampus: An overview of functional anatomy and protocol for their segmentation in MR images. In S. Ulmer & O. Jansen (Eds.), *FMRI: Basics and clinical applications* (pp. 355–383). Springer International Publishing. https://doi.org/10.1007/978-3-030-41874-8_24

Kivisaari, S. L., Tyler, L. K., Monsch, A. U., & Taylor, K. I. (2012). Medial perirhinal cortex disambiguates confusable objects. *Brain*, *135*(12), 3757–3769. https://doi.org/10.1093/brain/aws277

Krimer, L. S., Hyde, T. M., Herman, M. M., & Saunders, R. C. (1997). The entorhinal cortex: An examination of cyto- and myeloarchitectonic organization in humans. *Cerebral Cortex*, *7*(8), 722–731. https://doi.org/10.1093/cercor/7.8.722

Lace, G., Savva, G. M., Forster, G., de Silva, R., Brayne, C., Matthews, F. E., Barclay, J. J., Dakin, L., Ince, P. G., Wharton, S. B., & MRC-CFAS. (2009). Hippocampal tau pathology is related to neuroanatomical connections: An ageing population-based study. *Brain*, *132*(5), 1324–1334. https://doi.org/10.1093/brain/awp059

Levy, L. M., Henkin, R. I., Hutter, A., Lin, C. S., Martins, D., & Schellinger, D. (1997). Functional MRI of human olfaction. *Journal of Computer Assisted Tomography*, *21*(6), 849–856.

Llamas-Rodríguez, J., Oltmer, J., Greve, D. N., Williams, E., Slepneva, N., Wang, R., Champion, S., Lang-Orsini, M., Fischl, B., Frosch, M. P., van der Kouwe, A. J. W., & Augustinack, J. C. (2022). Entorhinal subfield vulnerability to neurofibrillary tangles in aging and the preclinical stage of Alzheimer's disease. *Journal of Alzheimer's Disease*, *87*(3), 1379–1399. https://doi.org/10.3233/JAD-215567

Maass, A., Berron, D., Libby, L. A., Ranganath, C., & Düzel, E. (2015). Functional subregions of the human entorhinal cortex. *eLife*, *4*, e06426. https://doi.org/10.7554/eLife.06426

Mai, J. K., Paxinos, G., & Voss, T. (2015). *Atlas of the human brain*. Academic Press.

Matej, R., Tesar, A., & Rusina, R. (2019). Alzheimer's disease and other neurodegenerative dementias in comorbidity: A clinical and neuropathological overview. *Clinical Biochemistry*, *73*, 26–31. https://doi.org/10.1016/j.clinbiochem.2019.08.005

Navarro Schröder, T., Haak, K. V., Zaragoza Jimenez, N. I., Beckmann, C. F., & Doeller, C. F. (2015). Functional topography of the human entorhinal cortex. *eLife*, *4*, e06738. https://doi.org/10.7554/eLife.06738

Nelson, P. T., Alafuzoff, I., Bigio, E. H., Bouras, C., Braak, H., Cairns, N. J., Castellani, R. J., Crain, B. J., Davies, P., Tredici, K. D., Duyckaerts, C., Frosch, M. P., Haroutunian, V., Hof, P. R., Hulette, C. M., Hyman, B. T., Iwatsubo, T., Jellinger, K. A., Jicha, G. A., … Beach, T. G. (2012). Correlation of Alzheimer disease neuropathologic changes with cognitive status: A review of the literature. *Journal of Neuropathology & Experimental Neurology*, *71*(5), 362–381. https://doi.org/10.1097/NEN.0b013e31825018f7

Nelson, P. T., Dickson, D. W., Trojanowski, J. Q., Jack, C. R., Boyle, P. A., Arfanakis, K., Rademakers, R., Alafuzoff, I., Attems, J., Brayne, C., Coyle-Gilchrist, I. T. S., Chui, H. C., Fardo, D. W., Flanagan, M. E., Halliday, G., Hokkanen, S. R. K., Hunter, S., Jicha, G. A., Katsumata, Y., … Schneider, J. A. (2019). Limbic-predominant age-related TDP-43 encephalopathy (LATE): Consensus working group report. *Brain*, *142*(6), 1503–1527. https://doi.org/10.1093/brain/awz099

Nilssen, E. S., Jacobsen, B., Fjeld, G., Nair, R. R., Blankvoort, S., Kentros, C., & Witter, M. P. (2018). Inhibitory connectivity dominates the fan cell network in layer II of lateral entorhinal cortex. *The Journal of Neuroscience*, *38*(45), 9712–9727. https://doi.org/10.1523/JNEUROSCI.1290-18.2018

Olsen, R. K., Carr, V. A., Daugherty, A. M., La Joie, R., Amaral, R. S. C., Amunts, K., Augustinack, J. C., Bakker, A., Bender, A. R., Berron, D., Boccardi, M., Bocchetta, M., Burggren, A. C., Chakravarty, M. M., Chételat, G., de Flores, R., DeKraker, J., Ding, S.-L., Geerlings, M. I., … Hippocampal Subfields Group. (2019). Progress update from the hippocampal subfields group. *Alzheimer's & Dementia (Amsterdam, Netherlands)*, *11*, 439–449. https://doi.org/10.1016/j.dadm.2019.04.001

Olsen, R. K., Palombo, D. J., Rabin, J. S., Levine, B., Ryan, J. D., & Rosenbaum, R. S. (2013). Volumetric analysis of medial temporal lobe subregions in developmental amnesia using high-resolution magnetic resonance imaging. *Hippocampus*, *23*(10), 855–860. https://doi.org/10.1002/hipo.22153

Ono, M., Kubik, S., & Abernathey, C. D. (1990). *Atlas of the cerebral sulci*. G. Thieme Verlag; Thieme Medical Publishers.

Palomero-Gallagher, N., Kedo, O., Mohlberg, H., Zilles, K., & Amunts, K. (2020). Multimodal mapping and analysis of the cyto- and receptorarchitecture of the human hippocampus. *Brain Structure & Function*, *225*(3), 881–907. https://doi.org/10.1007/s00429-019-02022-4

Pruessner, J. C., Köhler, S., Crane, J., Pruessner, M., Lord, C., Byrne, A., Kabani, N., Collins, D. L., & Evans, A. C. (2002). Volumetry of temporopolar, perirhinal, entorhinal and parahippocampal cortex from high-resolution MR images: Considering the variability of the collateral sulcus. *Cerebral Cortex*, *12*(12), 1342–1353. https://doi.org/10.1093/cercor/12.12.1342

Ritchey, M., Libby, L. A., & Ranganath, C. (2015). Cortico-hippocampal systems involved in memory and cognition: The PMAT framework. *Progress in Brain Research*, *219*, 45–64. https://doi.org/10.1016/bs.pbr.2015.04.001

Rose, M. (1927). Der Allocortex bei Tier und Mensch I. *Teil Journal of Psychology and Neurology*, *34*, 1–111.

Schön, M., Nosanova, A., Jacob, C., Kraus, J. M., Kestler, H. A., Mayer, B., Feldengut, S., Amunts, K., Del Tredici, K., Boeckers, T. M., & Braak, H. (2022). A comparative study of pre-alpha islands in the entorhinal cortex from selected primates and in lissencephaly. *The Journal of Comparative Neurology*, *530*(4), 683–704. https://doi.org/10.1002/cne.25233

Squire, L. R., & Zola-Morgan, S. (1991). The medial temporal lobe memory system. *Science (New York, NY)*, *253*(5026), 1380–1386. https://doi.org/10.1126/science.1896849

Stark, S. M., & Stark, C. E. L. (2016). The aging hippocampus: Linking animal and human research. In R. Cabeza, L. Nyberg, & D. C. Park (Eds.), *Cognitive neuroscience of aging: Linking cognitive and cerebral aging* (pp. 273–300). Oxford University Press. https://doi.org/10.1093/acprof:oso/9780199372935.003.0012

Stenger, S., Bludau, S., Mohlberg, H., & Amunts, K. (2022). Cytoarchitectonic parcellation and functional characterization of four new areas in the caudal parahippocampal cortex. *Brain Structure and Function*, *227*(4), 1439–1455. https://doi.org/10.1007/s00429-021-02441-2

Stephan, H. (Ed.). (1975). *Allocortex* (Vol. 4, p. 9). Springer. https://doi.org/10.1007/978-3-642-80890-6

Suzuki, W. A., & Amaral, D. G. (1994). Perirhinal and parahippocampal cortices of the macaque monkey: Cortical afferents. *Journal of Comparative Neurology*, *350*(4), 497–533. https://doi.org/10.1002/cne.903500402

Suzuki, W. A., & Amaral, D. G. (2003). Perirhinal and parahippocampal cortices of the macaque monkey: Cytoarchitectonic and chemoarchitectonic

organization. *Journal of Comparative Neurology*, *463*(1), 67–91. https://doi.org/10.1002/cne.10744

Swanson, L. W. (2003). *Brain architecture: Understanding the basic plan*. Oxford University Press.

Tahvildari, B., & Alonso, A. (2005). Morphological and electrophysiological properties of lateral entorhinal cortex layers II and III principal neurons. *Journal of Comparative Neurology*, *491*(2), 123–140. https://doi.org/10.1002/cne.20706

Taylor, K. I., & Probst, A. (2008). Anatomic localization of the transentorhinal region of the perirhinal cortex. *Neurobiology of Aging*, *29*(10), 1591–1596. https://doi.org/10.1016/j.neurobiolaging.2007.03.024

Tranel, D., Brady, D. R., Van Hoesen, G. W., & Damasio, A. R. (1988). Parahippocampal projections to posterior auditory association cortex (area Tpt) in old-world monkeys. *Experimental Brain Research*, *70*(2), 406–416. https://doi.org/10.1007/BF00248365

Van Hoesen, G. W., Augustinack, J. C., Dierking, J., Redman, S. J., & Thangavel, R. (2000). The parahippocampal gyrus in Alzheimer's disease: Clinical and preclinical neuroanatomical correlates. *Annals of the New York Academy of Sciences*, *911*(1), 254–274. https://doi.org/10.1111/j.1749-6632.2000.tb06731.x

Vandrey, B., Garden, D. L. F., Ambrozova, V., McClure, C., Nolan, M. F., & Ainge, J. A. (2020). Fan cells in layer 2 of the lateral entorhinal cortex are critical for episodic-like memory. *Current Biology*, *30*(1), 169–175. e5. https://doi.org/10.1016/j.cub.2019.11.027

von Bonin, G., & Bailey, P. (1947). *The neocortex of Macaca mulatta*. Univ. of Illinois Press.

von Economo, C., & Koskinas, G. N. (1925). *Die Cytoarchitektonik der Hirnrinde des erwachsenen Menschen*. J. Springer.

von Economo, C., & Koskinas, G. N. (1929). *The cytoarchitectonics of the human cerebral cortex*. Oxford University Press.

Williams, E. M., Rosenblum, E. W., Pihlstrom, N., Llamas-Rodríguez, J., Champion, S., Frosch, M. P., & Augustinack, J. C. (2023). Pentad: A reproducible cytoarchitectonic protocol and its application to parcellation of the human hippocampus. *Frontiers in Neuroanatomy*, *17*, 1114757. https://doi.org/10.3389/fnana.2023.1114757

Wisse, L. E. M., Daugherty, A. M., Olsen, R. K., Berron, D., Carr, V. A., Stark, C. E. L., Amaral, R. S. C., Amunts, K., Augustinack, J. C., Bender, A. R., Bernstein, J. D., Boccardi, M., Bocchetta, M., Burggren, A., Chakravarty, M. M., Chupin, M., Ekstrom, A., de Flores, R., Insausti, R., … Hippocampal Subfields Group. (2017). A harmonized segmentation protocol for hippocampal and parahippocampal subregions: Why do we need one and what are the key goals? *Hippocampus*, *27*(1), 3–11. https://doi.org/10.1002/hipo.22671

Xie, L., Wisse, L. E. M., Pluta, J., de Flores, R., Piskin, V., Manjón, J. V., Wang, H., Das, S. R., Ding, S.-L., Wolk, D. A., & Yushkevich, P. A. (2019). Automated segmentation of medial temporal lobe subregions on in vivo T1-weighted MRI in early stages of Alzheimer's disease. *Human Brain Mapping*, *40*(12), 3431–3451. https://doi.org/10.1002/hbm.24607

Yushkevich, P. A., Amaral, R. S. C., Augustinack, J. C., Bender, A. R., Bernstein, J. D., Boccardi, M., Bocchetta, M., Burggren, A. C., Carr, V. A., Chakravarty, M. M., Chételat, G., Daugherty, A. M., Davachi, L., Ding, S.-L., Ekstrom, A., Geerlings, M. I., Hassan, A., Huang, Y., Iglesias, J. E., … Zeineh, M. M. (2015). Quantitative comparison of 21 protocols for labeling hippocampal subfields and parahippocampal subregions in in vivo MRI: Towards a harmonized segmentation protocol. *NeuroImage*, *111*, 526–541. https://doi.org/10.1016/j.neuroimage.2015.01.004

Yushkevich, P. A., Muñoz López, M., Iñiguez de Onzoño Martin, M. M., Ittyerah, R., Lim, S., Ravikumar, S., Bedard, M. L., Pickup, S., Liu, W., Wang, J., Hung, L. Y., Lasserve, J., Vergnet, N., Xie, L., Dong, M., Cui, S., McCollum, L., Robinson, J. L., Schuck, T., de Flores, R., … Insausti, R. (2021). Three-dimensional mapping of neurofibrillary tangle burden in the human medial temporal lobe. *Brain*, *144*(9), 2784–2797. https://doi.org/10.1093/brain/awab262

Yushkevich, P. A., Pluta, J. B., Wang, H., Xie, L., Ding, S.-L., Gertje, E. C., Mancuso, L., Kliot, D., Das, S. R., & Wolk, D. A. (2015). Automated volumetry and regional thickness analysis of hippocampal subfields and medial temporal cortical structures in mild cognitive impairment. *Human Brain Mapping*, *36*(1), 258–287. https://doi.org/10.1002/hbm.22627

SUPPORTING INFORMATION

Additional supporting information can be found online in the Supporting Information section at the end of this article.

How to cite this article: Wuestefeld, A., Baumeister, H., Adams, J. N., de Flores, R., Hodgetts, C. J., Mazloum-Farzaghi, N., Olsen, R. K., Puliyadi, V., Tran, T. T., Bakker, A., Canada, K. L., Dalton, M. A., Daugherty, A. M., La Joie, R., Wang, L., Bedard, M. L., Buendia, E., Chung, E., Denning, A., … Wisse, L. E. M. (2024). Comparison of histological delineations of medial temporal lobe cortices by four independent neuroanatomy laboratories. *Hippocampus*, *34*(5), 241–260. https://doi.org/10.1002/hipo.23602